Science Front Publishers *Journal for Foundations and Applications of Physics*, **vol. 13, No. 1 (2026)**
(sciencefront.org) **ISSN 2394-3688**

A Testable Locally Real Representation of Quantum Mechanics in Agreement with Performed Experiments

Stuart Mirell[1,2,5*] and Daniel Mirell[3,4,5]

[1]Department of Radiological Sciences, University of California at Los Angeles, Los Angeles, California, USA
[2]Cyclotron Facility, VA GLAHS, Los Angeles, California, USA
[3]Department of Physics, University of New Mexico, Albuquerque, New Mexico, USA
[4]Department of Chemistry, University of California at Irvine, Irvine, California, USA
[5]Quantum Wave Technologies, Los Angeles, California, USA (current address)
**Corresponding author E-mail*: smirell@ucla.edu

(Received 21 March 2026, Accepted 08 August 2026, Published 24 August 2026)

Abstract

A locally real representation of quantum mechanics deduced from the underlying quantum formalism is presented here. The representation is based upon Mirell's local hidden variable theory, an LHVT, [doi:10.1103/PhysRevA.65.032102] that provides correlations in agreement with reported Bell experiments. Conversely, the non-local phenomenon of entanglement is necessarily invoked by the Copenhagen Interpretation of that formalism for those reported experiments by maintaining that the formalism is complete. Although a broad class of LHVT's has been disproven by Bell's inequality, Mirell's LHVT is identifiable as a special exempted case by its inherent inclusion of the property of enhancement. Clauser and Horne [doi:10.1103/PhysRevD.10.526] showed that LHVT's with the property of enhancement are not testable by Bell's inequality. In order to address that lack of testability, the representation presented here substantially expands on Mirell's earlier LHVT by self-consistently demonstrating locally real photon state transits of common loop configurations, transits that necessarily invoke non-local superposition under the Copenhagen Interpretation of the quantum formalism. We then analyze those locally real transits and deduce methods to re-engineer the loop configurations to achieve selected output state distributions and show that these re-engineered configurations are predicted by the present representation to yield novel distributions of locally real output states. Conversely, the Copenhagen Interpretation predicts corresponding output distributions for these re-engineered configurations that are unremarkable. Those mutually disparate output distributions provide the experimentally testable basis for definitively falsifying either the present locally real representation or the completeness of the original quantum formalism as postulated under the Copenhagen Interpretation.

Keywords: Enhancement, Non-local superposition, Entanglement, Local reality

1. Introduction

The underlying quantum mechanical formalism does not impose non-local phenomena. Rather, those phenomena are intrinsic to the widely accepted probabilistic interpretation commonly identified as the Copenhagen Interpretation "CI" of that underlying formalism. The non-local phenomena are attributed to particles and to photons in a variety of physical configurations as a necessary consequence of the positivist-based, compact CI.

This report proposes a locally real representation as an alternative to CI. The present representation, denoted as "LR," is based upon an earlier representation detailed in [1] that deduced locally real states of both photons and particles from the underlying quantum mechanical formalism, distinct from the Copenhagen Interpretation of that formalism. That earlier representation [1] demonstrated a locally real basis for phenomena that CI must represent as the non-local phenomenon of entanglement. The present LR representation substantially expands upon that demonstration by additionally showing a locally real basis for phenomena that CI necessarily represents as non-local superposition.

The LR representation is properly identifiable as a local hidden variable theory, LHVT. The variables that we identify here as essential to the LR representation arise naturally from the underlying quantum formalism. [1] LHVT's are widely perceived as being universally falsified by Bell's inequality [2] from the results of "Bell experiments" such as [3-4].

In [1] LR locally real states are examined in detail with respect to Bell experiments associated with correlated photon pairs and as well as with correlated particle pairs. In that examination the predicted LR-based outcomes for these experiments are nevertheless in agreement with outcomes of reported performed Bell experiments such as [3-4].

This agreement raises an apparent conundrum since LR, as an LHVT, would be expected to be falsified by those experiments. However, the LR representation inherently has the property of "enhancement" associated with correlated states. Significantly in this regard, Clauser and Horne deduced that LHVT's with the property of enhancement are not testable by Bell's inequality [5].

Beyond Bell experiments such as [3-4], related experiments have been devised and performed that test for "loopholes" which might falsely give the appearance of an LHVT in agreement with CI. In Genovese's comprehensive review [6] of hidden variable theories and reported experiments, the particular representation [1] is identified as an LHVT "not yet excluded by present experiments."

In the present report we focus on the LR states for photons and review the correlated photon experiments commonly associated with the general perception that the non-local phenomenon of entanglement is mandated by the outcomes of Bell experiments. The report further focuses on experiments relating to photon transits of common loop configurations such as Mach-Zehnder interferometers. Under CI, these loop experiments are commonly associated with the general perception that the phenomenon of non-local superposition is mandated by the outcomes of those experiments.

Specific expressions of CI for non-local superposition and entanglement can both be traced back to the CI specification for a linearly polarized state. The CI-based phenomenon of entanglement arises in processes such as an atomic system emitting a correlated pair of photons. When one photon of the pair is transmitted by a single channel polarizer preceding one of the detectors in a Bell experiment, that photon is specified by CI as being in a linearly polarized state upon interacting with that polarizer. With that polarizer's axis orientation defined as 0°, the state of the photon upon its interaction with the polarizer is more precisely identified by CI as a definite 0° linearly-polarized state. Accordingly, following that first photon's measurement by the first detector of a Bell experiment, the second photon of the pair, still in transit to the other Bell detector's polarizer, is then also in a definite 0° linearly polarized state from the perspective of CI, a perspective that imposes the non-local property of entanglement on the correlated pair.

In that process CI treats that second photon as a non-real, probabilistic entity until a measurement is performed. That second photon, now necessarily deemed to be in a probabilistic definite 0° linearly polarized state from the perspective of CI, has a $\cos^2\theta$ probability of being transmitted upon encountering an opposing, second polarizer rotated to some orientation θ relative to the first polarizer.

The CI-based phenomenon of non-local superposition also relates to the concept of a probabilistic linearly polarized state. When a probabilistic linearly polarized state photon is incident on a loop configuration, such as a polarizing beam splitter Mach-Zehnder interferometer, that state is split onto both legs of the loop. CI imposes the principle that the wave function of that incident state is a complete description of the state. In the case of a loop transit, that principle requires that the photon state must exist as a non-real probabilistic entity simultaneously on both legs of the loop. As a result, the state must be represented as a non-local superposition of the probabilistic state on both legs.

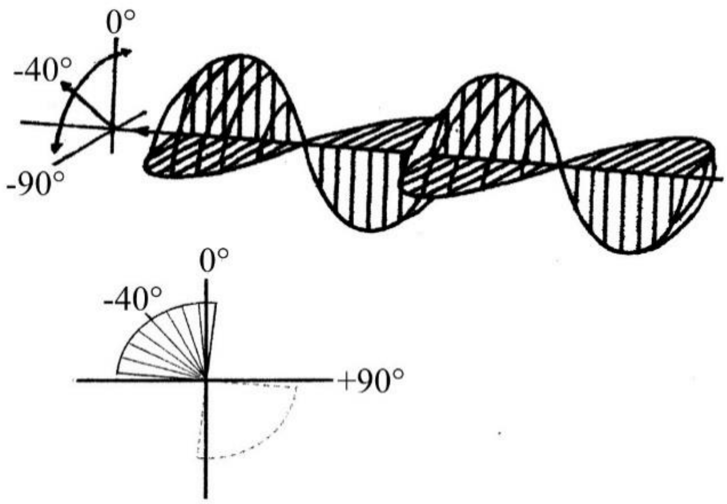

Fig. 1: An LR projective 3-dimensional view of a two-wavelength long segment of an objectively real linearly polarized photon wave packet with an orientation (arc bisector) at −40° as detailed in the accompanying transverse cross-sectional view. The depicted 90° transverse arc span is associated with an ordinary, full complement photon (as well as with the "generator" photon member of a correlated pair).

As an alternative to CI, we examine the consequences of treating photons as objectively real entities in the LR representation of states. [1] This treatment assigns to any single photon an objectively real wave structure. Deterministically, that wave structure prescribes the transmissibility of the photon through an encountered polarizer. These assignments have important consequences in the context of photons in linearly polarized states. In this report we specifically compare the CI and LR treatments of photons in linear polarization states. In cases for which CI necessarily invokes non-locality, we show that the LR treatment is unambiguously and self-consistently local. Moreover, the LR treatment elucidates physical processes that are occluded in the CI treatment from the perspective of LR.

We further examine the locally real states with particular regard for objectively real structural aspects of photon wave structure and interaction of that structure with polarizers. From the perspective of the LR representation, the ubiquitous CI linear polarization state associated with a photon exiting a simple linear polarizer, is no longer identified as a "state" representing a single photon. LR treats that CI "state" as a statistical "linear polarization ensemble" comprised of an infinite number of LR member states. Collectively, those member states yield the classic $\cos^2\theta$ transmission distribution as individual random members of the ensemble are each incident on a subsequent polarizer rotated by some θ relative to the previous polarizer. Each individual LR member of the ensemble has a characteristic orientation in the transverse plane that is deterministically predictive of its interaction outcome with a polarizer.

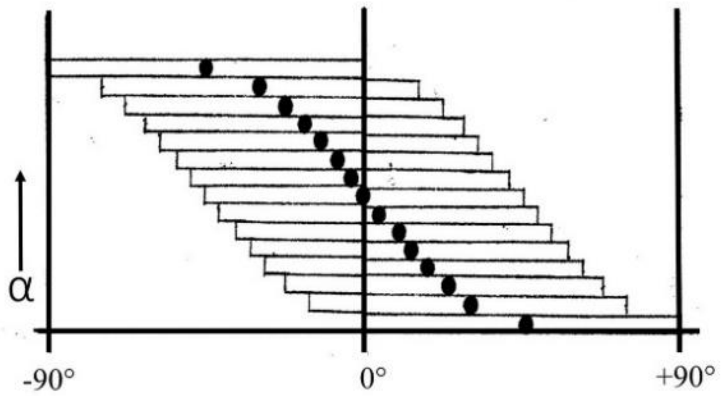

Fig. 2: A graphical representation of a 0° linearly polarized ensemble of LR photon waves, showing here for instructional purposes a finite 15-member ensemble. Each member (row) represents an ordinary wave with a transverse arc span of 90°. The arc bisectors of each member, denoted by arc-centered dots, are in a statistical cosine squared distribution relative to −45°. The ensemble members are designated by α=1→15 where α=1 corresponds to the bottom row.

Each individual LR state member of the linear polarization ensemble has an objectively real 3-dimensional structure, individually differentiated by the member's characteristic orientation. The longitudinal structure is equivalent to that underlying quantum formalism and the transverse structure is derived from that quantum formalism in [1]. Several wavelengths of the structure are depicted in Fig. 1.

The infinite member linear polarization ensemble can be satisfactorily approximated by a finite-member ensemble such as that depicted in Fig. 2 where each row represents the transverse arc span and relative transverse orientation of an individual locally real member state.

These 3-dimensional structures of individual locally real photon states self-consistently provide a locally real representation of phenomena fully in accord with the underlying quantum formalism where those phenomena are otherwise widely regarded as requiring a probabilistic, non-local representation.

2. Basics of the LR Locally Real Representation

A formal basis of the locally real representation LR was presented in [1] and presently relevant aspects of that basis are reviewed here. In that paper the basis was applied to locally real representations of correlated photons and correlated particles, phenomena that seemingly necessitate a non-real and non-local representation such as CI. A principal objective of the present paper is to apply [1] in a self-consistent manner to represent loop transits of photons which are also widely regarded as requiring a non-real and non-local representation such as CI. Accordingly, the LR basics presented here further include the self-consistent rules necessary to fully represent the photon states in those loop transits.

2.1. Geometric Structure of LR Photon States

LR is appropriately definable as a locally real “hidden variable theory,” LHVT. For photons, those “hidden variables” include variables that characterize the transverse wave packet structure. That structure is derived from first principles of the underlying quantum mechanical formalism and “completes” the three-dimensional representation of an objectively real wave packet. [1] LR, which inherently includes the property of enhancement, is not subject to Bell’s inequality [2], but is consistent with reported results of Bell experiments and CI predictions of those experiments such as in [3-4] and related experiments cited in [6].

Longitudinally, the objectively real wave structure of a photon is consistent with that given by the wave function ξ of the underlying quantum mechanical formalism. Transversely, that wave structure radially spans an arc Δ. Typically encountered photons have arc spans of 90° and are designated as ordinary or “full complement” photons. A notable exception includes atomic emission correlated pairs of photons where one member of each pair has an arc span $\leq 90°$. Photons with arc spans $<90°$ are designated as “partial complement” photons. A radial arc bisector defines the orientation of a particular photon. Fig. 1 illustrates a two-wavelength segment of an ordinary linearly polarized, full complement photon wave packet oriented at $-40°$ (and equivalently at $+140°$). An energy quantum associated with the photon resides at a point on that wave structure. The instantaneous locus of that energy quantum along the wave structure is mediated by the longitudinal wave function ξ.

This report primarily treats linearly polarized photons. Nevertheless, objectively real elliptically polarized photons are readily represented with LR states. An elliptically polarized wave packet in LR is a physically local superposition of two transversely orthogonal waves of the form associated with objectively real, linearly polarized photons and colinearly propagating. The respective amplitudes and the relative phase of the two wave forms determine the interaction properties of an elliptically polarized wave packet.

In this report for LR a "photon" is understood to comprise (at least) one point-like energy quantum and a wave packet. [1] That wave packet may be further identified as "occupied," in reference to that one or more energy quanta residing on it.

Conversely, in the absence of a resident energy quantum, a wave packet of a photon may be identified more concisely simply as a "wave" or more precisely as a "quantum wave" in the regard that an energy quantum can reside on such a wave. With no energy quantum present, that wave is said to be "unoccupied" or, equivalently, "empty."

Parenthetically we note that in the context of a wave packet, the associated wave is more precisely understood to be an integral over a distribution of pure wave states for LR consistent with the underlying quantum formalism and with CI.

2.2. Detailed Treatment of LR Locally Real Photon Wave States

In this subsection we examine the LR representation of the photon wave function with particular regard for presenting LR analyses of phenomenon that are necessarily identified as non-local superposition in CI. The treatment of correlated photons here and in [1] happens not to be dependent on the relative amplitude magnitudes of the photons in a correlated pair. However, in our present analyses of loop transits of single photon states which deal with an occupied wave and an unoccupied wave, the relative amplitude of those two waves is of consequence and is elevated to the level of an essential variable. In that regard we examine the photon wave function composition consistent with [1] and the associated wave function composition associated with beamsplitters which give rise to pair of objectively real waves, one occupied and one unoccupied.

In the context of the present analysis, in which interactions with devices such as polarizers are examined, the convention is followed here of using a highly compact form of the wave function that specifically treats those interactions. However, the notation used in this LR representation of wave functions is deliberately modified from that of CI in the interests of clearly distinguishing objectively real quantities from those of probabilistic quantities.

The analysis begins with a photon wave, effectively an occupied electromagnetic wave, propagating in free space or in a non-polarized medium. The photons we consider in this section are primarily "ordinary" linearly polarized photons, ordinary in the sense that they have "full complement" 90° transverse wave arcs as opposed to the exceptional case of "partial complement" photons with ≤90° wave arcs for one of the members in atomic emission correlated photon pairs At any point along the wave's propagation axis the amplitude is appropriately represented in the transverse plane by an infinite set of equal amplitude radial vectors uniformly distributed over the wave arc, 90° for full complement waves and ≤90° for partial complement waves. The resultant photon wave packet is a 3-dimensional structure modulated along the propagation axis by the longitudinal wave function ξ of the underlying quantum formalism schematically depicted in Fig. 1. [1]

2.2.1. The LR Wave Function

The uniform radial vectors that transversely define the arc of the wave packet arise from the derivation given in [1] for that structure. In that derivation the infinite basis vectors in Hilbert space are manifested as objectively real planar waves longitudinally represented by ξ and transversely by infinitesimal δ arc spans. These constituent planar waves are represented by an infinite set of $\boldsymbol{\varphi}_{\delta i}$ vector amplitudes, mutually identical except in their respective transverse radial orientations. Collectively, the contiguously arrayed planar waves constitute the Δ span of the wave packet. The transverse cross-sectional view included in Fig. 1 pictorially represents this infinite set of constituent planar waves by a finite set of eight radial partitions.

In view of this structure, the LR photon wave function is appropriately identified as a "multi-vector" amplitude state $\Sigma_i\boldsymbol{\varphi}_{\delta i}$ where the individual vector planar wave packets are represented by the $\boldsymbol{\varphi}_{\delta i}$ vector amplitudes. The summation $\Sigma_i\boldsymbol{\varphi}_{\delta i}$ constitutes a local superposition of the individual planar wave packet vector amplitudes. That multi-vector summation is compactly denoted here instead by $\underline{\boldsymbol{\Phi}}$, i.e. $\Sigma_i\boldsymbol{\varphi}_{\delta i} = \underline{\boldsymbol{\Phi}}$. The underscore is employed here to explicitly distinguish quantities such as $\underline{\boldsymbol{\Phi}}$ as multi-vector quantities.

When considering interactions of a photon wave with physical structures the multi-vector composition of $\underline{\boldsymbol{\Phi}}$ would seem to generally require a more cumbersome analysis than that with simple single vector quantities. However, the principal interactions we consider in this report concern projections of radial vector wave amplitudes onto a polarizer axis.

In that regard, it is fortuitous that for the symmetry of a vector set such as the $\boldsymbol{\varphi}_{\delta i}$, the sum of vectorial projections of a multiplicity of radial vectors onto a polarizer axis is equivalent to the vectorial sum of a multiplicity of radial vectors projected onto that polarizer axis. Additionally, the orientation of the vectorial sum of the vector set is equivalent to the arc bisector orientation of the vector set. These equivalences are applied further below in compactly treating polarizer interactions with simple vector quantities rather than with the encumbrances of multi-vector quantities.

When a multi-vector $\underline{\boldsymbol{\Phi}}$ wave amplitude is incident on a polarized medium a condensation process occurs that projects the angularly distributed constituent radial vectors onto the polarization axis of the polarized medium. These projections result in the 3-dimensional wave condensing to a 2-dimensional planar wave $\boldsymbol{\Phi}_\delta$ aligned with the medium's polarization axis in the transverse plane and modulated along the propagation axis by the longitudinal wave function ξ. In that process, the multi-vector $\underline{\boldsymbol{\Phi}}$ incident on the polarized medium transitions to a physically simple vector representation $\boldsymbol{\Phi}_\delta$ in the polarized medium. The δ subscript denotes that $\boldsymbol{\Phi}_\delta$ is a planar wave condensed from a multi-vector $\underline{\boldsymbol{\Phi}}$.

The multi-vector form of a wave function representing a wave propagating in free space wave or in a non-polarized transmissive medium is most generally

$$\underline{\boldsymbol{\Phi}}(\theta,z,t,\Delta,\omega)=\xi(z,t,\omega)\ m\ \underline{\mathbf{r}}(\theta,\Delta). \tag{1.2}$$

The arc span parameter Δ is included in this general expression for $\underline{\boldsymbol{\Phi}}$ in free space, however, we generally consider only common ordinary waves where Δ=90° and Δ can typically be omitted.

Similarly, the longitudinal wave function parameters z, t and ω can also be omitted in the context of most analyses presented in the present work where loop paths are optically equal. A minor exception occurs when one net 180° phase flip occurs on one loop path relative to the other path which introduces a negative sign on ξ for one path. Consequently, the compact form

$$\underline{\mathbf{\Phi}}(\theta)=\xi\, m\, \underline{\mathbf{r}}(\theta) \tag{2.2}$$

is generally sufficient in representing LR states.

The multi-vector $\underline{\mathbf{r}}(\theta)$ is a unit modulus, $|\underline{\mathbf{r}}(\theta)|=1$, transverse representation of $\underline{\mathbf{\Phi}}(\theta)$ similarly comprised of an infinite set of equal amplitude unit magnitude radial vectors uniformly distributed over a 90° arc (for an ordinary photon) with an arc bisector at θ. The longitudinal wave function is normalized to a unit modulus, $|\xi|=1$, so that the magnitude of $\underline{\mathbf{\Phi}}(\theta)$ is subsumed in some scalar amplitude coefficient m. That normalization is of particular utility when considering an amplitude $\underline{\mathbf{\Phi}}(\theta)$ split onto two paths 1 and 2. In such cases, the relative amplitude magnitudes of $\underline{\mathbf{\Phi}}(\theta)$ on the paths would be represented by m_1 and m_2, respectively, whereas the sinusoidal function ξ is the same for both paths. The value of θ denotes the objectively real bisector orientation in the transverse plane of the $\underline{\mathbf{\Phi}}(\theta)$ arc span.

The particular example of θ=0° (defined as the vertical axis) is first examined before proceeding to a general case of θ. When an objectively real $\underline{\mathbf{\Phi}}(0°)$ is normally incident on a polarizer with its polarization axis at 0°, the projections of the $\underline{\mathbf{r}}(0°)$ unit magnitude radial vectors along the 0° axis result in a narrow, large amplitude peak centered at the 0° polarization axis in a physical process mathematically analogous to that of the Dirac delta function.

Physically in that process of $\underline{\mathbf{\Phi}}(0°) \rightarrow \mathbf{\Phi}_\delta(0°)$, the squared modulus of the amplitude is conserved in further analogy to the Dirac delta function applied to the squared modulus of amplitudes over a wave packet condensing into a vanishingly narrow peak in the transverse plane. The wave function of $\mathbf{\Phi}_\delta(0°)$ is represented by

$$\mathbf{\Phi}_\delta(0°)=\xi\, M\, \mathbf{r}_\delta(0°) \tag{3.2}$$

where the δ subscript on the vector quantity $\mathbf{\Phi}_\delta(0°)$ explicitly denotes that the physical wave, which is now sharply peaked in the transverse plane, is appropriately physically representable as a vector quantity along the polarizer axis at 0°. In the transverse plane $\mathbf{\Phi}_\delta(0°)$ represents the condensation of some polarizer-incident multi-vector $\underline{\mathbf{\Phi}}$ which physically had extent over some finite arc span Δ in the transverse plane. The quantity $\mathbf{r}_\delta(0°)$ is the associated unit vector along the polarizer axis at 0° and the quantity M is the scalar amplitude magnitude coefficient of the $\mathbf{\Phi}_\delta$ vector amplitude. Within the polarizer, $\mathbf{\Phi}_\delta(0°)$ represents a planar wave propagating along the longitudinal axis while transversely aligned with the polarizer's axis at 0°.

2.2.2. Reduction of a Multi-vector to a Single Equivalency Vector

In analyzing transitions of the multi-vector amplitudes into and out of polarizers it is mathematically more expeditious if all constituent amplitudes of the $\underline{\mathbf{\Phi}}$ planar waves can be resolved to a simple single vector form. To this end, the "equivalency vector" $\mathbf{\Phi}$ is introduced here in mathematical replacement of the multi-vector $\underline{\mathbf{\Phi}}$ which more accurately physically represents waves in free space and in non-polarized mediums. Nevertheless, the equivalency vector $\mathbf{\Phi}$ still retains the properties necessary to represent amplitude interactions with polarizers while properly conserving its squared modulus in those interactions.

Then the multi-vector,

$$\underline{\mathbf{\Phi}}(0°)=\xi\, \mathrm{m}\, \underline{\mathbf{r}}(0°) \tag{4.2}$$

where its arc bisector unit vector is oriented at 0° in the transverse plane while in contrast the equivalency vector

$$\mathbf{\Phi}(0°)=\xi\, \mathrm{M}'\, \mathbf{r}(0°) \tag{5.2}$$

is represented in the transverse plane by a unit radial vector $\mathbf{r}$ oriented at 0° and the equivalency vector is scaled by a magnitude M′. In these respects the equivalency vector amplitude is mathematically similar to the physical δ-form vector amplitude Eq. (6.2) within a polarizer,

$$\mathbf{\Phi}_\delta(0°)=\xi\, \mathrm{M}\, \mathbf{r}_\delta(0°) \tag{6.2}$$

where 0° is necessarily the orientation of the polarization axis of the polarizer in which $\mathbf{\Phi}_\delta(0°)$ is propagating. For the equivalency vector $\mathbf{\Phi}(0°)$, that δ subscript is omitted as a reminder that unlike the δ-form vector, the equivalency vector is not physically a planar condensate but is instead a mathematical substitute for the polarizer-incident multi-vector $\underline{\mathbf{\Phi}}(0°)$.

The mathematical functionality of that substitution is made possible by the conservation of the squared modulus of the amplitude in the $\underline{\mathbf{\Phi}}(0°) \rightarrow \mathbf{\Phi}_\delta(0°)$ transition which allows, in a time reversal process, the imposition of the same magnitude onto the equivalency wave function $\mathbf{\Phi}(0°)$ as that on the planar wave function $\mathbf{\Phi}_\delta(0°)$ propagating within the polarizer, i.e. M′=M. Mathematically this imposes squared modulus conservation of the multi-vector $\underline{\mathbf{\Phi}}(0°)$ onto the equivalency vector $\mathbf{\Phi}(0°)$.

The above special case of θ=0° for waves incident on a polarizer can readily be extended to the general case of some objectively real θ for the multi-vector arc bisector orientation. For a multi-vector with an arc bisector at θ, the vector sum of the radial vectors is by symmetry a resultant vector that is oriented at θ. This allows a decomposition of an equivalency vector amplitude

$$\begin{aligned}\mathbf{\Phi}(\theta)&=\mathbf{\Phi}(0°)\cos\theta + \mathbf{\Phi}(90°)\sin\theta\\ &=\xi\, \mathrm{M}\cos\theta\, \mathbf{r}(0°) + \xi\, \mathrm{M}\sin\theta\, \mathbf{r}(90°).\end{aligned} \tag{7.2}$$

We then consider the above decomposed vector amplitude incident on a two-channel polarizer such as calcite where the "vertical" polarization axis is at 0° and the "horizontal" polarization axis is at 90°. Specifically, the equivalency vectors $\mathbf{\Phi}(0°)\cos\theta$ and $\mathbf{\Phi}(90°)\sin\theta$ are incident respectively on the polarizer's 0° and 90° axes. As a result, the δ-form amplitudes

$$\mathbf{\Phi}_\delta(0°)=\xi\, \mathrm{M}\cos\theta\, \mathbf{r}_\delta(0°) \tag{8a.2}$$

and

$$\mathbf{\Phi}_\delta(90°)=\xi\, M \sin\theta\, \mathbf{r}_\delta(90°) \qquad (8b.2)$$

respectively propagate on the 0° and 90° polarization channels. The squared moduli of these two δ-form amplitudes confirm that squared modulus values are conserved in this representation and demonstrates the utility of employing the equivalency vector in place of the multi-vector for the general case of a θ arc bisector.

Then in general the mathematically convenient equivalency vector expression for a multi-vector in free space or in a non-polarizing medium with an arc bisector at θ is given by

$$\mathbf{\Phi}(\theta)=\xi\, M\, \mathbf{r}(\theta). \qquad (9.2)$$

In summary, there are three principal amplitude wave vector forms that are commonly utilized in LR:

1. $\underline{\mathbf{\Phi}}(\theta)$ and $\underline{\mathbf{r}}(\theta)$ are multi-vectors that physically correspond to the transverse geometry of LR waves in free space and in non-polarizing media.

2. $\mathbf{\Phi}(\theta)$ and $\mathbf{r}(\theta)$ are "equivalency" vectors that can be used as simplified mathematical vector substitutes for multi-vector representations of waves in free space and in non-polarizing media in computing interactions with polarizers.

3. $\mathbf{\Phi}_\delta(\theta)$ and $\mathbf{r}_\delta(\theta)$ are vector quantities that physically and mathematically correspond to δ-form planar waves propagating in a polarizer and in alignment to a polarization axis of the polarizer.

2.2.3. Energy Quantum Transfers Associated with Wave Amplitudes Incident on Polarizers

The outcome of energy quanta on waves incident on polarizers must also be addressed in the context of the wave functions. Below we continue the above generalization of polarizers to two-channel devices with a "vertical" polarization axis at 0° and a "horizontal" polarization axis at 90° as we track the transfers of energy quanta.

The transfer of energy quanta of the wave onto a channel of a polarizer is deterministically dependent upon the wave's incident arc intersecting that channel. That condition is determined from the equivalency vector orientation θ which is the orientation of the actual arc bisector of the 90° arc span of the "ordinary" photon wave packets we are considering here. If θ is such that $-45°<\theta<+45°$, the 90° transverse arc of the mode wave structure intersects the 0° vertical polarization axis and any energy quanta that occupy the wave are confined to the vertical polarization channel of the polarizer as the radial vectors of the wave projectively condense along the vertical polarization axis. Effectively in this process, the energy quantum is "trapped" onto a planar wave propagating in alignment with the vertical polarization axis. Concurrently, there is still a projection onto the incident wave amplitude onto the horizontal axis that results in a planar wave propagating in alignment with the horizontal axis of the polarizer but that horizontally oriented planar wave is empty.

Conversely for an incident state with an orientation θ where +45°<θ<+135° the above process is reversed and energy quanta on that incident state are confined to the polarizer's horizontal polarization channel as an occupied planar wave and the associated planar wave aligned to the polarizer's vertical axis is empty.

For the objectively real "ordinary" photons we consider here, i.e. with full complement 90°arc spans, the arc bisector orientation of any incident photon can be objectively specified as some θ. For the special cases of vertically polarized or horizontally polarized photons, −45°<θ<+45° or +45°<θ<+135°, respectively. Note that for the special case of correlated photons where the arc span may be a partial complement less than 90°, that arc span may intersect neither polarization axis and the energy quantum is absorbed in the polarizer.

The presence of energy quanta on a wave amplitude is indicated by a "+" subscript. For example, the equivalency vector amplitude

$$\mathbf{\Phi}(\theta)_+ = \xi\, M\, \mathbf{r}_\delta(\theta)_+ = \xi\, \mathbf{r}(\theta)_+ \tag{10.2}$$

is occupied and has a unit modulus when M=1.

For the case of −45°<θ<+45°, when $\mathbf{\Phi}(\theta)_+$ is incident on a two-channel polarizer, the projective condensation of that amplitude onto the vertical polarization axis along with the energy quantum residing on the wave packet arc results in an occupied δ-form vector amplitude

$$\mathbf{\Phi}_\delta(0°)_+ = \xi \cos\theta\, \mathbf{r}_\delta(0°)_+ \tag{11a.2}$$

propagating on the vertical polarization channel with a magnitude cos θ. Then, deterministically,

$$\mathbf{\Phi}_\delta(90°) = \xi \sin\theta\, \mathbf{r}_\delta(90°) \tag{11b.2}$$

is the vector amplitude propagating on the horizontal polarization channel with a magnitude |sin θ|. Since −45°<θ<+45°, the associated arc of the incident wave does not intersect the horizontal axis and the vector amplitude propagating on the horizontal polarization channel $\mathbf{\Phi}_\delta(90°)$ is an "empty" wave as indicated by the absence of a "+" subscript.

It may be appreciated that analyses utilizing $\mathbf{\Phi}(\theta)_+$ equivalency vectors rather than $\underline{\mathbf{\Phi}}(\theta)_+$ multi-vectors are more expedient for purposes of wave calculation. However, energy quantum transfers onto a particular polarization axis require that we separately take into account the implicit arc span associated with those equivalency amplitude vectors. Nevertheless, this concern is generally trivial because essentially all arc spans of waves are 90° unless they are associated with waves of correlated photons in which case we must also take into account the statistical distribution of objectively real arc spans for correlated photons.[1]

2.2.4. Detailed Examination of Linear Polarization Ensembles

There are numerous occasions encountered in the analyses presented here in which we consider a CI probabilistic definite linear polarization "state" such as that associated with θ-polarized photons. Consistent with CI, each of those photons is said to be in that definite state and each photon is associated with the familiar cosine squared probability curve centered at some specified angle which we can choose as 0°. Of particular interest are the probability computations for transmission of those definite state photons through a polarizer with an axis at some orientation θ. The transmission probability for those definite state photons is computed from the magnitude of the probability curve evaluated at the angular separation $\theta - 0°$ between the probability curve's center and the polarizer's axis. The result is simply $\cos^2\theta$. The cosine squared curve is deliberately left with unit normalization to maintain consistency of that curve as a mathematical probability that ascends to a value of 1 as $\theta \to 0°$.

This treatment of the definite state photons is fully self-consistent with the positivist-based CI that treats the photon as a probabilistic entity. The probability curve functionally yields the correct proportion of observable polarizer transmissions for definite state photons. For the probabilistic photons no causal mechanism is offered or admitted for the well-known observed proportion of transmissions as a function of polarizer axial orientation.

Conversely, from the perspective of LR, the CI probabilistic definite state, linearly polarized at some orientation such as 0°, is not the state of a single photon but is instead a statistical representation of an ensemble of objectively real photon states. Those states are depicted in Fig. 2 for the 0° linear polarization ensemble where the 15-member ensemble is an approximation to the objectively real infinite-member ensemble.

A 0°-linear polarization ensemble of photons can be generated by directing randomly oriented photons at a polarizer with its axis oriented at 0°. Half of those photons successfully propagate in the polarizer as δ-form waves and reach the exit face of the polarizer. At that face each successive photon wave that is emitted has the orientation of a random member (row) of the Fig. 2 0°-linear polarization ensemble.

Accordingly, the orientation of any emitted photon wave is independent of the particular orientation of the incident photon wave from which the emitted wave is derived. The orientation of an incident photon might properly be interpreted as being "lost" in that process. However, information regarding the arc bisector orientation of the incident photon is present on the δ-form wave as an amplitude cofactor derived from the vector projection of that orientation on the polarizer axis. That cofactor is retained as an objectively real variable on the amplitude of the objectively real photon wave emitted from the polarizer exit face with an orientation of a random member of the 0°-linear polarization ensemble.

Diagrammatically, each LR objectively real photon wave is represented by one of the ensemble members, e.g. one of the rows in the Fig. 2 distribution. The process is identifiable as "stochastic." The orientation of a particular member is given by the orientation of the arc bisector of that member where each member has a 90° arc span. Most generally, that arc bisector orientation is specified here by adopting the convention that θ_α denotes the orientation of the α member of a θ-centered LR polarization ensemble. The subscript is given by a lower-case Greek letter (other than δ to avoid confusion with δ-form waves) or an integer if a specific member of an ensemble distribution is to be identified.

As an example of this convention, in the Fig. 2 finite-member approximation of a 0°-polarized ensemble, $0°_\alpha$ specifies that the objectively real LR wave state is transversely represented by the arc bisector orientation for member α in the depicted 0°-polarization ensemble where the index α is numerically 1→15 beginning with the lowest depicted row as α=1. In this case $0°_1$ is +45°. The arc bisector orientations (the loci of the dots centered on each row) map to a cosine squared curve for the members on the right side of the distribution and to a vertically inverted cosine squared curve for the members on the left side of the distribution. That mapping provides for members that are statistically representative of the polarization ensemble distribution in a finite-member approximation. The Fig. 2 distribution is derived from first principles of the underlying quantum mechanical formalism. [1]

From this LR perspective the usual cosine squared curve is not treated as a probability distribution of a definite state photon. Rather, from a modified distribution such as that in Fig. 2, the distribution is understood to graphically represent the objectively real transverse wave arcs of a statistically representative "polarization ensemble" of LR member photon states. If a polarizer is positioned to intercept the member states, a vertical line at any θ on the Fig. 2 distribution represents the polarizer's axial orientation at that θ. The polarizer's axis intersects a $\cos^2\theta$ fraction of those member wave arcs resulting in that fraction of ensemble members being transmitted by the polarizer together with any resident energy quanta. Accordingly, for any 0°-polarization ensemble of photons a $\cos^2\theta$ fraction is causally the mathematical transmission probability for any random member being transmitted by the polarizer rotated to θ.

If waves from a photon source incident on a polarizer are identified as "vertically" polarized, in LR that implies that the orientations θ of the waves are statistically that of random members of a vertical polarization ensemble as depicted in Fig. 2 using a finite-member ensemble for instructional purposes.

If the photon source directs these waves at a polarizer, where the axis of the full ensemble is in alignment with the polarizer's axis, defined as the vertical axis 0°, then an individual source wave, i.e. an ensemble member, has an orientation $0°_\alpha$ where α is some random number 1 to 15. That particular axial alignment has important consequences. From Fig. 2, the arcs of all the ensemble members intersect the polarizer's vertical polarization axis. As a result, for any particular wave of those 15 the energy quantum on the wave transitions onto the vertically oriented polarizer axis along with the cosine projection of the incident wave amplitude. That incident amplitude from the source can be expressed as

$$\mathbf{\Phi}(0°_\alpha)_+=\xi\,\mathbf{r}(0°_\alpha)_+ \tag{12.2}$$

which is in a normalized form with a unit modulus since the magnitude M=1. The appended subscript "+" denotes that the wave amplitude is occupied which identifies Eq. (12.2) as representing an amplitude of a photon.

The amplitude in the polarizer's vertical channel is

$$\mathbf{\Phi}_\delta(0°)_+=\xi\cos(0°_\alpha)\;\mathbf{r}_\delta(0°)_+ \tag{13.2}$$

which retains the energy quanta that had resided on the incident $\mathbf{\Phi}(0°_\alpha)_+$ but has a reduced wave amplitude as a result of the cosine projection of the α wave onto the polarizer's vertical axis.

2.2.5. Malus's Law with Regard to CI and LR States

Malus's law, dating back to 1808, is a statistical rule of light transmission through a polarizer that can be understood as an underlying basis for the CI treatment of a definite photon polarization state as a probabilistic construct. For CI a 0°-polarized definite state is prepared by directing unpolarized photons to a first polarizer with its polarization axis oriented at 0° where that orientation is defined as "vertical." A subsequent, second polarizer, with its axis set to various θ orientations, promptly yields the $\cos^2\theta$ transmission distribution of Malus's law. From the positivist-based CI, all the definite polarization state photons emerging from the first polarizer are mutually indistinguishable prior to their respective interactions with the second polarizer and all are regarded as identical entities. At any particular θ′ setting of the second polarizer's axis, the relative $\cos^2\theta'$ transmission probability for those identical photons is treated as an expression of an inherent property of all of those photons. In that context, the photons are necessarily classified as probabilistic entities.

Conversely for LR, a causal basis of Malus's $\cos^2\theta$ transmission distribution is trivially demonstrated by the Fig. 2 LR linear polarization ensemble. Consider for example an orientation of the second polarizer's axis at some $\theta' > 0°$. A vertical line at that θ′ on Fig. 2 intersects a fraction of the arcs of the ensemble members which would deterministically result in the transmission of those members. That fraction is simply $\cos^2\theta'$. Since the distribution of objectively real orientations for the photons emitted from the first polarizer is the same as the Fig. 2 polarizer ensemble distribution, Malus's law is demonstrated for $\theta' > 0°$ and, by symmetry, for $\theta' < 0°$ as well.

2.2.6. The LR States in a Definite Linear Polarization Ensemble

The LR linear polarization ensemble statistically represents the objectively real states of a definite polarized state. When an incident photon is successfully transmitted in a polarizer that ensemble is generated at the exit face of the polarizer and a random member of the ensemble is emitted. The linear polarization ensemble consists of an infinite-member set, each with a 90° arc span, and with orientations (arc bisectors) defined by a cosine squared curve centered at the orientation of the emitting polarizer's axis. The above phenomenon regarding a state emerging from a polarizer constitutes an important first rule of polarizer emission from the perspective of LR.

RULE 1 of polarizer emission: A wave state emerging from a polarizer unaccompanied by an orthogonal wave state is emitted as a random member of a linear polarization ensemble centered at the orientation of the polarizer's axis.

In most of the discussions below, "ensemble" refers to the ubiquitous "linear polarization ensemble" unless otherwise specified. (A notable exception considered further below is the "correlated photon ensemble" that relates to LR states of photons defined by CI as "entangled.")

The equation

$$\theta_\alpha = \cos^{-1}[(\alpha-1)/(N-1)]^{1/2} - (\theta+45°) \tag{14.2}$$

is the general representation of a finite-member polarization ensemble, giving the bisector orientations for a finite number N of ensemble members where the ensemble is centered at the θ orientation. In Eq. (14.2) the finite-member ensemble is represented by the quantity θ_α where θ is the orientation of the polarization ensemble and the values of α, $1\rightarrow N$, identify the individual members with α=1 corresponding to the lowest row.

For the particular Fig. 2 ensemble where θ=0° and N=15, Eq. (14.2) takes the form

$$0°_\alpha=\cos^{-1}[(\alpha-1)/14]^{1/2}-45°. \tag{15.2}$$

The finite-member ensemble illustrated in Fig. 2 assigns a unique orientation from an equation such as Eq. (15.2) that properly preserves the relative frequency distribution of constituent states. It can readily be appreciated that a vertical axis applied to the Fig. 2 distribution at some angular orientation θ transects a $\cos^2\theta$ fraction of the arc spans. With that vertical axis physically representing the polarization axis of a one-channel polarizer intercepting the arc spans of random members of the ensemble, we see that a well-defined $\cos^2\theta$ fraction of the members are deterministically transmitted by the polarizer. In this graphic representation of a member distribution, the arc bisectors of a finite set of members are mapped one-to-one onto the orientation associated with each of the respective members. In the limit as $N\rightarrow\infty$, an ensemble such as that depicted in Fig. 2 converges to an infinite-member ensemble that precisely represents a physical linear polarization ensemble.

However, for a finite member polarization ensemble, as in Fig. 2, the respective member orientations are determined by the numerical choice of N in an equation such as Eq. (14.2). As a practical matter, it is useful to further identify this type of ensemble as a finite-member "numerically partitioned" linear polarization ensemble in recognition of the basis by which the ensemble envelope is partitioned into individual members.

An instructive and useful alternative to that type of ensemble is constructed from a uniform angular partitioning of space. The resultant finite-member "angularly partitioned" linearly polarized ensemble is generated from the derivative of the arc-bisector curve given by

$$B(\theta)=\cos^2(\theta+45°) \tag{16.2}$$

for a physically precise infinite-member 0° linear polarization ensemble. Eq. (16.2) is recognized as the right-hand envelope boundary of the ensemble translated to the left by 45° thereby bisecting each of the N-infinite members. The derivative of B(θ),

$$\partial_\theta B(\theta)=-\sin[2(\theta+45°)] \tag{17.2}$$

is proportional to $\Delta N/\Delta\theta_i$ which is a function of θ_i. The $\Delta\theta_i$ are a set of uniform angular partitions of space applied in the transverse plane, where each partition has the same angular span $\delta=|\Delta\theta_i|$ centered at the θ_i. ΔN is the fraction of N members associated with a particular $\Delta\theta_i$ partition. This relationship accurately holds for small δ together with finite but suitably large N giving a finite-member ensemble that trivially converges to a precise representation of an actual physical ensemble as $\delta\rightarrow0°$.

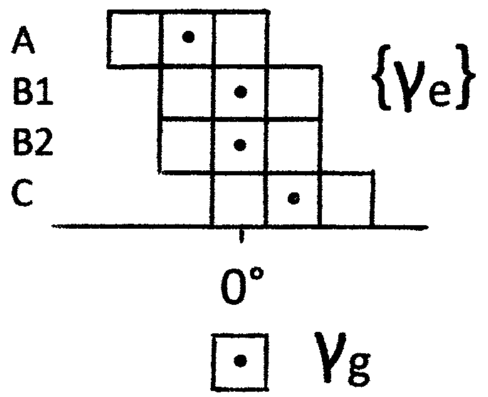

Fig. 3: A four-member, angularly partitioned polarization (emission) ensemble $\{\gamma_e\}$ symbolically and functionally representing a 0°-linear polarization ensemble. This figure additionally includes the planar state γ_g from which $\{\gamma_e\}$ is generated.

Conversely, as δ increases to macroscopic angular partitions, exact proportionality of $\Delta N/\Delta\theta_i$ to $\partial_\theta B(\theta)$ degrades. Nevertheless, at a very coarse δ=30° the resultant angularly partitioned ensemble is remarkably useful. A mere four members provide a complete set for the δ=30° partition ensemble that retains functional equivalence to the corresponding actual physical ensemble at the θ_i's of the partition ensemble. Additionally, because of these functional equivalences, the four-member, δ=30° partition-based ensemble is symbolically utilized below in representation of actual physical ensembles.

Fig. 3 depicts that four-member, angularly partitioned, 0°-linear polarization ensemble identified as the set of "emission" photons $\{\gamma_e\}$ where the four members are individually identified as A, B1, B2, and C to facilitate tracking of each state in the process of various ensemble interactions. This finite member angularly partitioned ensemble is substantially a representational alternative to the Fig. 2 numerically partitioned polarization emission ensemble also symbolically denoted as $\{\gamma_e\}$.

The "generator" photon γ_g in Fig. 3 identifies the planar wave photon in the polarizer that gives rise to the ensemble $\{\gamma_e\}$ at the exit face of the polarizer from which a random member is emitted. Notably, the generator photon γ_g, transversely occupying a finite 30° partition in the Fig. 3 partition-based ensemble, properly converges to its actual physical infinitesimal planar δ-form in the limit as $\delta \to 0°$. It can be appreciated that the joint symbolic use of "δ" in representing the angular span of a partition as well as the infinitesimal angular span of a planar wave is appropriate in this limit.

The instructive utility of the angularly partitioned ensemble arises from mathematical symmetries that occur between functions such as $\cos^2\theta$ and angular partitions such as 30° where the function assumes rational values that can be represented by a small integral number of states.

In our examination of correlated photon pairs, subsection **3.1** further below, we will encounter a correlated photon emission ensemble functionally represented by a sin 2θ envelope. Fortuitously, that function similarly assumes rational values for 30° angular partitions which similarly facilitates a useful angularly partitioned ensemble representation with a mere two states.

For the Fig. 3 angularly partitioned ensemble, the transmission outcome of each individual member is fully deterministic with respect to a subsequent polarizer oriented to the partition orientations ±90°, ±60°, ±30° and 0°. For the entire four-member ensemble, a polarizer oriented to the complete set of partition orientations, −90°, −60°, −30°, 0°, +30°, +60°, and +90°, yields respective transmission factors of 0/4, 1/4, 3/4, 4/4, 3/4, 1/4, and 0/4 after applying the normalization required for a four-member ensemble. These transmission factors give exact agreement for this definite linear polarization state at those seven partition orientations.

The finite-member Fig. 2 numerically partitioned ensemble and the Fig. 3 angularly partitioned ensemble both converge to an infinite-member ensemble in their respective limits, N→∞ and δ →0°. Both finite-member ensemble constructions are useful in the analyses below concerning the relationship of CI definite polarization states and LR locally real states. These types of finite-member ensembles are also relevant to the analysis below of CI correlated states in relation to LR locally real states. Both types of finite-member ensembles are instructively useful in graphically depicting LR phenomena with countable states. Nevertheless, each type is separately advantageous in particular contexts and, accordingly, one of those types is selectively utilized to that advantage in the various contexts of the sections below.

Importantly, we stress here that quantities such as $\underline{\mathbf{\Phi}}(\theta)$, its equivalency representation $\mathbf{\Phi}(\theta)$, and the planar representation $\mathbf{\Phi}_\delta(\theta)$ are individual LR states that are not representable in CI notation. Moreover, a state such as $\mathbf{\Phi}(\theta_\alpha)$ with a subscripted orientation denotes an LR state that has the orientation of the α member of a polarization ensemble centered at θ. The LR state $\mathbf{\Phi}(\theta_\alpha)$ should not be confused with a CI state explicitly representing a definite θ-polarized state such as the ket $|\theta\rangle$. From the perspective of LR, a definite linearly polarized "state" in CI is a probabilistic set of individual objectively real $\mathbf{\Phi}(\theta_\alpha)$ LR states with a frequency distribution given by a polarization ensemble centered at θ.

The CI treatment of a definite linear polarization state as a complete representation, irreducible into individual constituent states such as the $\mathbf{\Phi}(\theta_\alpha)$ in LR, is a critical factor in the necessity of CI invoking non-locality in photon loop transits.

2.2.7. The Relationship of LR Wave States to Electromagnetic Waves, Maxwell's Equations and Fresnel Equations

In the LR analyses of photons transiting devices such as polarizers, outcomes are repeatedly shown to be mediated by the device interactions with photon quantum waves and not by the energy quanta that may or may not reside on the photon wave packets. Objectively, in these transits, when a wave packet is incident on a device such as a non-polarizing beamsplitter, a polarizing beam splitter, or a calcite polarizer, the resultant properties of the wave on an output of that device are independent of the incident wave packet being occupied or empty.

The apparent wave-like entity of an electromagnetic "wave" may then be more properly appreciated as a quantum wave populated by a multitude of energy quanta. An electromagnetic wave is perceived to be a wave-like entity only because the smoothly varying sinusoidal physical interactions of a multitude of energy quanta encountering macroscopic structures obfuscate the underlying graininess of the individual energy quanta interacting with those macroscopic structures. That graininess is made manifest when the electromagnetic wave is reduced to its elemental form of an occupied wave packet, i.e. a photon.

The underlying relationship of locally real occupied and empty wave states to electromagnetic waves can be understood from Maxwell's equations. Those equations show that a propagating wavelike entity exhibiting electromagnetic properties can exist and that the wave can carry energy. Historically, the subsequent understanding that resident photon energy quanta are responsible for the electromagnetic properties and energy of those waves serves to further validate Maxwell's electromagnetic waves. It should be noted, however, that while Maxwell's equations clearly allow a propagating electromagnetic entity, those equations do not exclude or even relate to the possibility that such a wave can exist devoid of those electromagnetic properties and energy. This is a relevant consideration from the perspective of local reality because at the level of individual quanta on a wave, a splitting of that wave by various beam splitters necessitates the existence of an empty wave.

In the interests of completeness we briefly examine here the phenomenon in which empty waves are generated and how those waves are transformed into "electromagnetic waves." To this end we consider the example of a simple dipole antenna that, when driven by an oscillatory current at some particular frequency ω, generates a characteristic dipole 3-dimensional electromagnetic wave emanating from the antenna. We begin our examination with a very low antenna driving current. Under the oscillatory acceleration of electrons along the antenna, the vacuum field surrounding the antenna undergoes corresponding coherent oscillatory perturbations from the spatially extended distribution of accelerated electrons.

From the perspective of local reality those distributed perturbations respectively generate mutually interfering empty wavelets with a resultant fully formed characteristic dipole 3-dimensional empty wave propagating out from the antenna notably as an empty wave and not as an "electromagnetic wave." Dissipative radiative energy associated with the oscillatory acceleration of any of the electrons along the antenna can be transferred to that outgoing empty wave only when an available energy reaches $\hbar\omega$ sustainable by the wave oscillatory at ω. For a very low driving current that transfer event is relatively rare and, when it occurs, a solitary "photon" may be detected at some point on the wavefront.

Nevertheless, if we are patient and sample over 4π with detectors, the solitary events would eventually still paint a point-like image of a characteristic dipole radiation field. At these very low current levels, if we could objectively visualize the wave, it would appear to be a complete 3-dimensional dipole wave, virtually empty except for occasional energy quanta propagating outward from the antenna as solitary photons in a spatial distribution consistent with the characteristic dipole field geometry.

As the driving current is increased the wave amplitude increases everywhere and the number of occasional energy quanta populating the wave also increases. At still higher currents, the wave amplitude substantially increases along with the number of energy quanta and the emanating wave is densely populated with energy quanta simultaneously at all points of the characteristic dipole wave.

We turn now to the CI representation of this example. At the very low currents singular quantum energy emission events are still expected to occur and might seem to cause a dilemma. A singular emission event at some point along the antenna does not generate the same resultant wave geometry as that of simultaneous multiple emissions from the physically extended charge distribution along the physical extension of the antenna. Over time, 4π detector sampling of these singular events would not map to the characteristic dipole field geometry.

The probabilistic CI readily circumvents this dilemma by noting that we have no knowledge of where on the antenna that emission occurs. The event could have occurred at any point along the antenna. As a consequence, the collective probabilistic wavelets emanating from the multiplicity of points along the antenna mutually interfere to generate the characteristic wave geometry of the physically extended accelerated charge distribution which, in the present example, is a 3-dimensional dipole wave geometry. The singular radiative emission event can successfully transfer energy to that outgoing wave in the amount of $\hbar\omega$.

In this interpretation the probabilistic dipole wave is the wave-like embodiment of the particle-like emission energy quantum $\hbar\omega$. It should be noted that non-locality is inherent in this CI representation at this level of singular events to the extent that spatially separated points along the antenna must simultaneously emit probabilistic wavelets at those points. That non-locality is obfuscated for higher driving currents where multiple emissions do statistically occur at spatially separated points along the antenna.

Certainly, the CI representation of non-locality in this example of photon emission does not rise to the explicit expression of non-locality seen in loop transits of photons. However, we include this example in the interests of further illuminating the role of empty waves in local reality. In this present example at very low antenna driving currents the pervasive empty waves deterministically exhibit the smoothly varying well-defined outgoing wave geometry of a complete dipole radiation field without the presence of the energy quanta.

In effect that outgoing empty wave precedes any energy quanta that are transferred from the antenna to the empty wave by increasing the antenna driving current. From this perspective, the ability to populate an empty wave with energy quanta that exhibit electromagnetic phenomena is consistent Maxwell's equations which demonstrate that such electromagnetic phenomena can propagate on a wave.

Importantly, the deterministic role of the wave itself in the above emission example is repeated throughout the analyses below. In these analyses the disposition of individual energy quanta at devices such a beamsplitters are repeatedly shown to be causally determined from the quantum waves deterministically traversing those devices.

The LR states may be understood as linguistic expressions of the quantum waves and not the energy quanta that may reside on the waves. Linguistically, the appropriate insertions of energy quanta onto those expressions are determined from context.

Classic two slit interference provides an instructive example of causal determination of energy quanta disposition by waves that is of particular relevance in the above examination of a weakly driven dipole antenna source. If the current driving the dipole antenna is sufficiently small, virtually no energy quanta are emitted but nevertheless a substantially complete 3-dimentional dipole radiation field of empty waves is still generated.

To perform the classic two slit interference experiment with this source a screen with a single small slit aperture is positioned near the antenna. The slit transmits a collimated beam of empty wave radiation slightly angularly dispersed by diffractive phenomena at the slit. A second screen equipped with two closely positioned small slits is placed at a short distance beyond the first screen such that the beam spot of that collimated beam is substantially incident on both slits. Each of the two resultant beams respectively exiting the two slits are further slightly angularly dispersed by diffraction at those two slits. An "observation" screen is placed at some distance in the far field where that diffractive dispersal causes the beams from the two slits to substantially overlap.

Objectively there is a distinctive well-defined interference pattern in that far field distance. The interference pattern is deterministically generated by the pervasive, real empty waves even in the total absence of energy quanta. The pattern is slowly visualized by incrementally increasing the antenna current to produce occasional quantum emission events. Those individual energy quanta enter a pre-existing empty wave interference field and unremarkably are causally concentrated in regions of constructive wave interference at the observation screen.

The consequential deterministic effects of empty waves also relate to basic physical laws such as the Frensel equations. Those equations seemingly relate specifically to electromagnetic waves traversing devices such as beamsplitters and should be re-examined. An inspection of the derivation of the Frensel equations immediately shows that the equation results are entirely dependent on relative electromagnetic wave amplitudes and not on energy related interactions of those waves. The Frensel equations can be self-consistently derived entirely from the quantum wave amplitudes of locally real states independent of the presence or absence of energy quanta on those states. From this independence we can deduce that empty waves and occupied waves both interact identically with dielectrics such as those in non-polarizing beam splitters, polarizing beam splitters and mirrors.

The foregoing observations from the perspective of LR are instructive in demonstrating that there is no fundamental profound transition in going from a microscopic "quantum realm" to a macroscopic "classical realm." In the above examples the only process that may be appropriately characterized as a characteristic "quantum mechanical" phenomenon occurs at the onset of energy quanta on the antenna ascending from the antenna onto the empty wave envelope emerging from the antenna. That onset occurs when the antenna driving current is sufficient to generate local radiative dissipation energy at points along the antenna to the quantum threshold of $\hbar\omega$ for coherent ascension of those energy quanta onto the existing ω-frequency empty wave.

2.3. Interactions of Locally Real states with Non-polarizing and Polarization-based Beamsplitters

For the locally real representation, the magnitude of the correlated photon arc span and the orientation of that arc's bisector constitute the sufficient "hidden" variables needed in analyzing the correlated photon phenomenon. In the present report we review the locally real representation of the correlated photon phenomenon and also examine locally real representations of photon loop transits. These representations follow directly and self-consistently from ref. [1].

Loop transits commonly involve devices that divide photon waves onto two paths. In that process, from a locally real perspective, a real occupied wave travels on one path and a real unoccupied empty or that for these loop transits the unoccupied wave travels on the other path. We show relative wave amplitude magnitudes on the two paths, in addition to arc span and arc bisector orientation, constitute the requisite complete set of variables necessary for formulating an LR devoid of non-local phenomena. The detection of a photon on one path has no influence on the wave amplitude of the other path. (In loop examples presented in this report it is understood that the optical path lengths are equivalent.)

Conversely for CI, in an interaction of a probabilistic photon with a beam splitting device, when the photon is detected on one of the output paths, the probability wave on that path is instantaneously elevated to a unit probability and the probability wave on the other path is simultaneously non-locally collapsed to zero. That process is necessary to maintain consistency with the CI principle that the photon wave function is a complete representation of the probabilistic photon inclusive of wave-like and particle-like (energy quantum) properties.

2.3.1. Transits of LR Wave States in Non-polarizing Beamsplitters

The simplest device for beam splitting is the non-polarizing beamsplitter which divides an incident wave into two similar structures. With respect to the r reflection and t transmission coefficients, the amplitudes of the reflected wave and the transmitted wave are each deterministically reduced relative to the incident wave by factors of the r and t moduli, respectively.

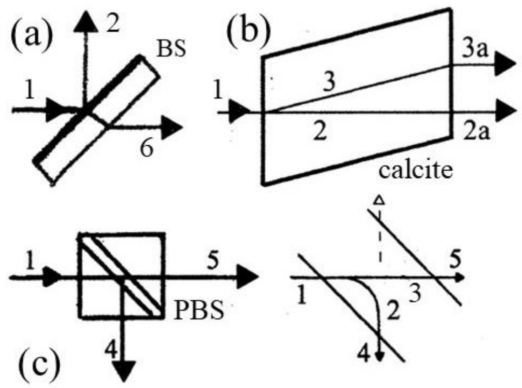

.**Fig. 4:** Beamsplitters and transits of locally real states. (a) Non-polarizing beamsplitter with dielectric front surface (b) Polarization-based calcite crystal beamsplitter (c) Polarizing beam splitter PBS depicted with detail of the diagonal dielectric layer. In (b) and (c) the vertical polarizer axis is perpendicular to the plane of the figures and the horizontal axis lies in the plane of the figures.

Other than amplitude reduction, the two waves emerging from a non-polarizing beamsplitter are structurally identical to that of the incident photon wave including the properties of arc span and arc bisector orientation. The energy quantum on the incident wave transfers to the reflected or the transmitted wave with a mathematical probability proportional to the squared moduli of their respective amplitudes.

The equations

$$\mathbf{\Phi}_1(\theta)=\xi 1\mathbf{r}(\theta)\rightarrow_{\text{BS-r}} \mathbf{\Phi}_2(\theta)= -\xi r\mathbf{r}(\theta) \tag{18.2}$$

and

$$\mathbf{\Phi}_1(\theta)=\xi 1\mathbf{r}(\theta)\rightarrow_{\text{BS-t}} \mathbf{\Phi}_6(\theta)=\xi t\mathbf{r}(\theta) \tag{19.2}$$

deterministically represent the waves of LR states respectively reflected and transmitted at the beam splitter aside from the particular disposition of the energy quantum for any incident LR state $\mathbf{\Phi}_1(\theta)$ on path 1 of Fig. 4(a). The incident state has some arc bisector orientation θ that is maintained in this beam splitting process. For interactions with non-polarizing beamsplitters the similarity of the waves for LR states $\mathbf{\Phi}_2(\theta)$ and $\mathbf{\Phi}_6(\theta)$ relative to that of the incident $\mathbf{\Phi}_1(\theta)$ is also maintained with respect to arc span Δ. Although, for virtually all states we consider in this report other than those of correlated emission photons, Δ=90°. We commonly assign an incident state $\mathbf{\Phi}_1(\theta)$ a unit normalized amplitude magnitude. In the present example of a non-polarizing beamsplitter, that assignment conveniently results in the subsequent amplitude magnitudes expressed entirely as the moduli of the r reflection and the t transmission coefficients.

Consistent with Fig. 4(a), Eq. (18.2) shows a negatively signed longitudinal wave function $-\xi$ relative to that of Eq. (19.2). That negative sign represents a 180° longitudinal phase flip due to the incident $\mathbf{\Phi}_1(\theta)$ reflecting off the first surface dielectric with a transparent substrate under that dielectric layer. In the context of the present report, which primarily treats the transverse aspects of wave functions, the longitudinal wave function ξ is generally not relevant. Phase flips, however, represent an exception to the extent that the negative sign in these cases is properly associated with the longitudinal wave function. Nevertheless, in loop analyses where only the relative phase on the two legs is consequential, equal net phase flips on both legs can be ignored.

Eq's. (18.2) and (19.2) are incomplete to that extent that if the incident state $\mathbf{\Phi}_1(\theta)$ represents a "photon," i.e. an occupied wave $\mathbf{\Phi}_1(\theta)_+$, the presence of an energy quantum is not indicated nor is the mathematically probabilistic outcome of the energy quantum transitioning to either $\mathbf{\Phi}_2(\theta)$ or $\mathbf{\Phi}_6(\theta)$. If for example the incident state is occupied and that energy quantum transition occurs onto $\mathbf{\Phi}_2(\theta)$, Eq. (18) can be completed to the form

$$\mathbf{\Phi}_1(\theta)_+ = -\xi 1\mathbf{r}(\theta)_+ \rightarrow_{\text{BS-r}} \mathbf{\Phi}_2(\theta)_+ = -\xi r\mathbf{r}(\theta)_+. \tag{18a.2}$$

Conversely, if the incident state $\mathbf{\Phi}_1(\theta)$ is unoccupied, Eq's. (18.2) and (19.2) would stand as complete.

2.3.2. Transits of LR Wave States in Calcite Beamsplitters

We consider a photon state represented by $\mathbf{\Phi}_1(\theta)_+$ at normal incidence on a calcite polarizer as depicted in Fig. 4 (b). The photon encounters two orthogonal axes, an axis designated as the "vertical polarization axis" defined as 0° and an orthogonal axis designated as the "horizontal polarization axis" defined as 90°.

We first treat the case in which the arc of that incident photon wave intersects the vertical axis. That intersection criterion is satisfied by any LR member oriented at θ of a vertically oriented linear polarization ensemble where $-45° < \theta < +45°$, which in CI is associated with a definite 0° linear polarization "state." That θ orientation can be represented as $0°_\mu$. The complete transit of the photon through the polarizer for this case is represented by the sequence of LR occupied states

$$\mathbf{\Phi}_1(0°_\mu)_+ = \xi\, \mathbf{r}_1(0°_\mu)_+ \rightarrow_{\text{cal-v}}$$

$$\mathbf{\Phi}_{\delta 2}(0°)_+ = \xi \cos 0°_\mu\, \mathbf{r}_\delta(0°)_+ \rightarrow_{\text{pol-emis}}$$

$$\mathbf{\Phi}_{2a}(0°_\alpha)_+ = \xi \cos 0°_\mu\, \mathbf{r}(0°_\alpha)_+. \tag{20.2}$$

Because of the intersection of the transverse arc with the calcite polarizer's vertical axis the transverse arc of the $\mathbf{\Phi}_1(\theta)_+$ wave projectively condenses along the vertical axis of the calcite polarizer and the wave propagates in the polarizer as a planar vertically oriented 2-dimentional wave on the path 2 colinear to that of the incident photon on path 1. In that condensation process, the energy quantum is trapped onto the planar wave in the polarizer. The condensation process is a vector projection of the incident photon amplitude in forming the planar wave. That projection confers a $\cos 0°_\mu$ coefficient to the planar wave amplitude $\mathbf{\Phi}_{\delta 2}(0°)_+$.

When that planar wave reaches the exit face of the polarizer, the planar wave generates and emits a conventional 3-dimentional wave with a "full-complement" arc, a 90° arc span, that has an arc bisector orientation statistically associated with that of a random member of a vertical linear polarization ensemble centered on the polarizer's vertical axis. The orientation of that random member is represented by $0°_{\alpha}$.

Because we are presently considering the case in which there is intersection of the incident photon's arc with the vertical axis, the 2-dimensional vertically oriented planar wave and the associated emitted 3-dimensional wave are occupied. The magnitude of the amplitude of the emitted, occupied photon wave is equivalent to that of the incident photon diminished by the cos $0°_{\mu}$ coefficient.

Concurrent with the above process associated with the intersected vertical polarization axis, a similar process occurs at the non-intersected orthogonal horizontal polarization axis. That process is summarized by the sequence

$$\mathbf{\Phi}_1(0°_{\mu})_{+}=\xi\ \mathbf{r}(0°_{\mu})_{+} \rightarrow_{\text{cal-h}}$$

$$\mathbf{\Phi}_{\delta 3}(90°)=\xi \sin 0°_{\mu}\ \mathbf{r}_{\delta}(90°) \rightarrow_{\text{pol-emis}}$$

$$\mathbf{\Phi}_{3a}(90°_{\beta})=\xi \sin 0°_{\mu}\ \mathbf{r}(90°_{\beta}) \tag{21.2}$$

Importantly, although the condensation of incident wave arc in the presently considered case does not trap the energy quanta onto the horizontal axis, there is a complementary projection of the incident photon's amplitude onto the horizontal axis. In that process the projection confers a sin $0°_{\mu}$ amplitude coefficient to an empty horizontal planar wave amplitude.

For calcite, the trajectory of the horizontal planar amplitude refracts by at an angle of 6.2° degrees within the crystal but otherwise emerges normal to the crystal exit face where the planar wave generates and emits a conventional 3-dimentional empty wave with a "full-complement" arc, a 90° arc span, that has an arc bisector orientation statistically associated with that of a random member of a horizontal (90°) linear polarization ensemble centered on the polarizer's horizontal axis. The magnitude of the amplitude of the emitted, empty photon wave $\mathbf{\Phi}_{3a}(90°_{\beta})$ is equivalent to that of the incident photon diminished by the sin $0°_{\mu}$ coefficient.

That emitted random β ensemble member is uncorrelated to the emitted random α ensemble member at the vertical axis because the two emission processes are non-local to each other. The non-correlation of the two emission processes is explicitly represented by the different member indices α and β.

In the alternate case of the horizontal polarization axis intersecting the arc of the incident photon, an occupied photon wave emerges from the horizontal axis exit point and an empty photon wave emerges from the vertical axis exit point but otherwise the magnitudes of the amplitudes and the assignment of orientations are consistent with the first case.

There are three final cases to be considered. The first two relate to incident correlated photon waves and the third relates to incident waves that are not photons but are instead empty photon waves.

For correlated photons if the arc span of the incident photon is less than 90° and the arc span does intersect one of the polarizations axes, e.g. the vertical axis, the outcome would proceed as described above in Eq. (21.2). However, in that process the information that the incident photon had an arc span $\Delta<90°$ is lost. The output state has a larger arc span of $\Delta=90°$ and the detectability of that photon is effectively "enhanced" relative to the incident photon in that process which increases the photon's wave cross section. [1] and [5]

For correlated photons, if the arc span of the incident photon is less than 90°, it is possible that the arc of the photon intersects neither polarization axis of the calcite. In this case the energy quantum is absorbed in the crystal and empty waves are emitted from the crystal exit points of both axes.

Alternatively, if the incident wave is empty, that wave may be represented by $\mathbf{\Phi}_1(0°_\mu)$. In this case, even though a wave arc may intersect one of the calcite axes, no energy quantum is present and empty photon waves are emitted from the crystal exit points of both axes.

In both of the above final cases, the magnitudes and orientations of the two empty wave amplitudes are nevertheless consistent with the previously examined cases in which an occupied state is emitted at one of the outputs of the calcite polarizer. Accordingly, these two final cases are still properly represented by the sequences Eq's. (20) and (21) but devoid of the "+" subscripts that indicate the presence of energy quanta.

2.3.3. Transits of LR Wave States in PBS Polarizing Beamsplitters

The analysis of an LR state traversing a polarizing beam splitter PBS, depicted in Fig. 4(c) is very similar to that for a calcite polarizer. We begin with a case analogous to that first examined above for the calcite polarizer in which the incident photon wave packet arc intersects the vertical axis of a PBS. Consistent with the above assignment of axis orientations, the vertical axis of a PBS relates to the reflected wave on path 4. The corresponding horizontal axis relates to the transmitted wave on path 5.

In comparing the calcite polarizer and the PBS we note that there is an important physical distinction that bears on the nature of the respective pairs of output states. For the calcite polarizer the interaction zone, where the incident state $\mathbf{\Phi}_1$ is split into the two planar states $\mathbf{\Phi}_{\delta 2}$ and $\mathbf{\Phi}_{\delta 3}$, is nonlocal to the two mutually non-local interaction zones at the exit face of the polarizer where $\mathbf{\Phi}_{\delta 2}$ emerges as $\mathbf{\Phi}_{2a}(0°_\alpha)$ and where $\mathbf{\Phi}_{\delta 3}(\theta)$ emerges as $\mathbf{\Phi}_{3b}(90°_\beta)$, respectively. In contrast, for the PBS all three analogous zones are mutually local in the dielectric layer of the PBS. The depicted thickness of that layer is greatly exaggerated in Fig. 4(c) for clarity in schematically showing the planar wave paths 2 and 3 within the dielectric layer.

Aside from the difference in the respective localities of the interaction zones, the wave transit analysis for the PBS is nearly identical to that of the calcite polarizer. With that simplification we can adopt the properly amended the sequence of amplitudes of the previous subsection before considering the ramifications of interaction locality in the PBS.

The properly amended sequence of amplitudes for the PBS are

$$\mathbf{\Phi}_1(0°_\mu)_+ = \xi\, \mathbf{r}(0°_\mu)_+ \rightarrow_{\text{PBS-v}}$$

$$\mathbf{\Phi}_{\delta 2}(0°)_+ = \xi \cos 0°_\mu\, \mathbf{r}_\delta(0°)_+ \rightarrow_{\text{pol-emis}}$$

$$\mathbf{\Phi}_4(0°_\alpha)_+ = \xi \cos 0°_\mu \, \mathbf{r}(0°_\alpha) \tag{22.2}$$

for the incident amplitude reflection at the PBS dielectric and

$$\mathbf{\Phi}_1(0°_\mu)_+ = \xi \, \mathbf{r}(0°_\mu)_+ \rightarrow_{\text{PBS-h}}$$

$$\mathbf{\Phi}_{\delta 3}(90°) = \xi \sin 0°_\mu \, \mathbf{r}_\delta(90°) \rightarrow_{\text{pol-emis}}$$

$$\mathbf{\Phi}_5(90°_\beta) = \xi \sin 0°_\mu \, \mathbf{r}(90°_\beta). \tag{23.2}$$

for the incident amplitude transmission through the PBS dielectric. Here, as with the transit analysis for the calcite polarizer, we consider without loss of generalization an incident state oriented at some orientation θ where $-45°<\theta<+45°$ and express that orientation as $0°_\mu$.

For the PBS the three final cases concerning totally empty output waves examined above in subsection **2.3.2.** for the calcite polarizer similarly apply to the PBS. Moreover, as with the calcite polarizer transits, the PBS output wave amplitudes are independent of the presence or absence of an energy quantum on the incident wave and the above equations similarly apply for an empty incident wave.

Because of the locality of the interaction processes for the PBS, the wave transit is seen as a unitary process. The implications of that conjecture can be evaluated by applying time reversal TR of the Eq.'s (22.2) and (23.2) amplitudes and inspecting the output amplitude. The time-reversed sequences up to the juncture of path 1 at the dielectric layer are

$$\mathbf{\Phi}_{4\text{-TR}}(0°_\alpha)_+ = \xi \cos 0°_\mu \, \mathbf{r}(0°_\alpha)_+ \rightarrow_{\text{PBS-v}}$$

$$\mathbf{\Phi}_{\delta 2\text{-TR}}(0°)_+ = \xi \cos 0°_\mu \cos 0°_\alpha \, \mathbf{r}_\delta(0°)_+ \tag{22a.2}$$

and

$$\mathbf{\Phi}_{5\text{-TR}}(90°_\beta) = \xi \sin 0°_\mu \, \mathbf{r}(90°_\beta) \rightarrow_{\text{PBS-h}}$$

$$\mathbf{\Phi}_{\delta 3\text{-TR}}(90°) = \xi \sin 0°_\mu \sin 90°_\beta \, \mathbf{r}_\delta(90°). \tag{23a.2}$$

Then at that juncture the orientation of the resultant vectorial sum of the two planar amplitudes $\mathbf{\Phi}_{\delta 2\text{-TR}}(0°)_+$ and $\mathbf{\Phi}_{\delta 3\text{-TR}}(90°)$ is the orientation of the time-reversed output state $\mathbf{\Phi}_{1\text{-TR}}$. That orientation, given by

$$\tan^{-1}[(\sin 0°_\mu \sin 90°_\beta)/(\cos 0°_\mu \cos 0°_\alpha)] = 0°_\mu \tag{24.2}$$

only when $\alpha=\beta$. With that condition the resultant time-reversed "incident" state

$$\mathbf{\Phi}_{1\text{-TR}}(0°_\mu)_+ = \xi \cos 0°_\mu \, \mathbf{r}(0°_\mu)_+ \tag{25.2}$$

is deterministically identical to the incident state $\mathbf{\Phi}_1(0°_\mu)_+$ diminished in wave amplitude by the factor $\cos 0°_\mu$.

For this time-reversed process the diminished amplitude of $\mathbf{\Phi}_{1\text{-TR}}$ does not constitute lost amplitude. The missing amplitude on $\mathbf{\Phi}_{1\text{-TR}}$ can be traced to the respective transmission projection of $\mathbf{\Phi}_{4\text{-TR}}(0°_\alpha)_+$ and the reflection projection of $\mathbf{\Phi}_{5\text{-TR}}(90°_\beta)$ at the PBS dielectric producing a resultant empty state exiting from the PBS dielectric on the unnumbered dashed path. In this regard a unitary process in the context of LR implies conservation of orientation but does not ensure that amplitude magnitude is conserved on a particular state for which orientation is conserved. Overall, in a time-reversed process, the squared moduli of the amplitude magnitudes are conserved.

A principal objective here in the context of the time-reversal analysis is to demonstrate that under a unitary process there is a local correlation of $\alpha=\beta$ that occurs in the PBS dielectric. That local correlation should however be recognized as a physically imposed phenomenon. Emission states from a polarizer output channel have orientations of random members of the associated polarization ensemble by **RULE 1**. That rule still applies to the $\mathbf{\Phi}_4(0°_\alpha)_+$ and $\mathbf{\Phi}_5(90°_\beta)$ states emitted from separate output channels of the PBS dielectric. However, the evolution of the two states within a common local zone physically requires the mutual orthogonality of those states within that local zone while simultaneously still having orientations of a random member of their respective polarization ensembles. That mutual orthogonality under these conditions is achieved by the local correlation $\alpha=\beta$ and Eq. (23.2) is revised to the sequence

$$\mathbf{\Phi}_1(0°_\mu)_+=\xi\,\mathbf{r}(0°_\mu)_+ \rightarrow_{\text{PBS-h}}$$

$$\mathbf{\Phi}_{\delta 3}(90°)=\xi \sin 0°_\mu\,\mathbf{r}_\delta(90°) \rightarrow_{\text{pol-emis}}$$

$$\mathbf{\Phi}_5(90°_\alpha)=\xi \sin 0°_\mu\,\mathbf{r}(90°_\alpha). \tag{23b.2}$$

It may then be appreciated that conservation of orientation is the effect of the present unitary process and the physical necessity of the local correlation is the cause of the present unitary process.

An additional objective in the present time-reversal analysis is to introduce a second rule of emission states from a polarizer.

RULE 2 of polarizer emission: Orthogonal wave states of the same wavelength mutually exiting at a common point from respective outputs of a two-channel polarizer combine deterministically to emit their vectoral resultant.

This 2nd rule complements the 1st rule which relates to an unaccompanied state exiting from an output channel of a polarizer with the orientation of a random member of a polarization ensemble.

2.3.4. Probability, Deterministic Processes, and Random Processes

A more complete examination of probability as well as of associated deterministic and random processes has been deferred to this point because those topics are most clearly understood after having first examined wave state interactions with devices such as non-polarizing and polarization-based beam splitters.

We begin with the CI wave state of an individual photon. The amplitude modulus is necessarily set to unity consistent with the principle that the photon wave function is the complete representation of the photon. The resultant representation of the photon which follows from that principle necessitates that the entity of the photon be treated as a probability and, as such, that probability must be shown to be conserved. Loosely speaking, that objective is commonly achieved by imposing a unit amplitude modulus on a photon and requiring that the squared modulus, i.e. the wave intensity, is still unit valued. To demonstrate probability conservation in the course of interactions where the photon might be split onto separate paths, the associated separated squared moduli are shown to sum to unity.

Utilizing the amplitude moduli in this manner to demonstrate probability conservation is certainly expedient and is generally correct. Nevertheless, we want to briefly examine the underlying formal demonstration of probability conservation for CI so that we can similarly also rely on that more expedient method of simply calculating squared amplitude moduli in demonstrating a corresponding property of (mathematical) probability conservation in LR.

For the photon, the total probability is calculated by first determining expression for the squared moduli at all points along the wave packet and then spatially integrating that expression over the entire wave packet. In many circumstances such as loop transits, the longitudinal wave function is essentially identical in amplitude moduli at all respective common points along the separated wave packets aside from a predictable amplitude coefficient acquired in transit of a beam splitting device at entry to the loop.

Then it may be appreciated that the ratio of the computed probabilities for the separated photon wave packets is equal to the ratio of the squared moduli for any arbitrary corresponding points along those separated wave packets. The outcome of interactions of those separated wave packets when combined at the loop terminus can be predicted by the ratio of the packet's respective probabilities but, based upon the above considerations, we can instead justifiably rely on the equivalent ratio of the squared moduli associated with any corresponding points along the separated wave packets. This expeditious simplification is appropriate for CI and is also applied to LR where photons are not probabilistic entities but where the objectively real integrated squared moduli of a wave packet are similarly also conserved quantities.

To that end in LR we identify the quantity of integrated squared moduli over a wave packet, which is equivalently the integrated wave intensities over that wave packet, as "ΣI" in symbolic representation of a summation of intensities. ΣI is an objectively real quantity and is effectively the LR analog to the term probability in CI where that term is applied as an expectation measure of a non-real entity as opposed to a mathematical likelihood.

Wave transits for beamsplitters in the present section and for loops in subsequent sections repeatedly demonstrate that ΣI is a conserved wave quantity for individual LR states totally independent of the energy quanta that might reside on those wave states in contrast to CI where probability conservation is inherently attached to the observable measurement of an energy-bearing photon. That demonstration for LR is expeditiously facilitated indirectly, as in CI, from readily available values of squared moduli on loop configurations. Importantly, no collapse of ΣI quantities is invoked or occurs in LR.

In the course of LR analyses in this report we routinely assign a unit normalized amplitude modulus to objectively real incident states purely for convenience in tracking subsequent fractional departures from that unit value as various interactions with devices occur. That assignment can be appreciated as mathematically equivalent to arbitrarily assigning a ΣI=1 for that incident state. In contrast for CI, that unit-valued modulus for the incident probabilistic state is necessitated by the initial wholeness of that incident state's probability. In any case, that common convention of adopting a unit amplitude modulus for incident states simplifies a comparison of LR and CI states after subsequent interactions modify those states.

In our examination of non-polarizing beamsplitters in subsection **2.3.1**, the squared output amplitude moduli (the wave intensities) from Eq's. (18.2) and (19.2) are respectively $|\mathbf{\Phi}_2(\theta)|^2=r^2$ and $|\mathbf{\Phi}_6(\theta)|^2=t^2$ which for an ideal non-polarizing beamsplitter sum to unity. Accordingly, for this simple example we can infer that the integrated wave intensity ΣI is conserved.

Notably in LR, this outcome demonstrates that the interaction of the incident wave with the non-polarizing beamsplitter is a fully deterministic process with respect to the outgoing wave intensities of the reflected and transmitted waves. However, in the context of outgoing waves for the non-polarizing beamsplitter we are faced with an indeterminate assignment of a resident energy quantum on the incident wave onto one or the other of the outgoing waves. In self-consistent resolution of that assignment for LR we turn to an adaptation of Born's first assumption.

In that adaptation we first consider a propagating wave packet not interacting with any devices such as a beamsplitter. Born's first assumption effectively tells us that a resident energy quantum at any point along the wave packet statistically migrates to neighboring points mediated by the relative local mathematical probability in the dτ spatial neighborhood of those points. For example, along the propagation axis z an energy quantum instantaneously at a point z_0 between two neighboring points z_{-1} and z_{+1} is subject to the sinusoidal variation of the squared modulus of the longitudinal wave function $|\xi(z_{-1})|^2$ and $|\xi(z_{+1})|^2$ at those two neighboring points which confer the respective proportional variations onto the local neighboring probabilities $|\mathbf{\Phi}(\theta,z_{-1})|^2\, d\tau_{-1}$ and $|\mathbf{\Phi}(\theta,z_{+1})|^2\, d\tau_{+1}$. (Here we are reminded that our otherwise consistent normalization of the modulus $|\xi|$ was applied to a $\mathbf{\Phi}$ represented at a particular longitudinal point and not to $\mathbf{\Phi}$'s represented at different longitudinal points along a wave packet.)

These considerations for migration of an energy quantum can be applied to the non-deterministic process of assigning that energy quantum onto the emerging reflected and transmitted fractions of the wave packet at the beamsplitter surface. Significantly, in that process migration onto those fractions is independent of the sinusoidal variations associated with ξ because the non-polarizing beamsplitter interaction leaves the two outgoing waves virtually identical to each other and to the incident wave, changing only the relative propagation directions of the outgoing reflected and transmitted waves as well as conferring respective r and t amplitude coefficients. Then initial points mutually equidistant from the beamsplitter surface on the outgoing reflected path 2 and transmitted path 6 have identical magnitudes of ξ on the two paths in the respective local neighborhoods of those points at $d\tau_r$ and $d\tau_t$. The only distinction between the relative local neighboring mathematical probabilities on those initial points are shown by

$$|\mathbf{\Phi}(\theta)_2|^2\, d\tau_r = r^2 d\tau_r \tag{26a.2}$$

and

$$|\mathbf{\Phi}(\theta)_6|^2\, d\tau_t.= t^2 d\tau_t. \tag{26b.2}$$

In the context of these expressions, Born's first assumption justifiably directs us to objectively randomly assign migration of the energy quantum onto the reflected and the transmitted waves of the non-polarizing beamsplitter in respective proportions of r^2 and t^2.

In contrast, wave transits of a calcite polarizer treated previously in subsection **2.3.2** present a substantial departure from wave transits of a non-polarizing beamsplitter. From Eq's. (20.2) and (21.2) we still see conservation of ΣI deduced from the respective output state squared moduli of each. At incidence the appropriate path that must be assigned for the energy quantum on an incident state such as $\mathbf{\Phi}_1(0°_\mu)_+$ is deterministically mandated by the orientation (and arc span) of that objectively real incident state. For the present example of an incident state $\mathbf{\Phi}_1(0°_\mu)_+$, the orientation $0°_\mu$ signifies that an "ordinary" 90° arc span necessarily intersects the vertical axis of the calcite. (If the arc span were <90° and the arc did not intersect the vertical axis, the energy quantum would be absorbed by the crystal.) When the arc, intersected by the vertical axis, condenses as it enters the polarizer, a resident energy quantum on that is arc is trapped onto the vertical axis in that process. The same condensation process would occur for a simple plate polarizer that has a single polarization axis similarly designated as vertical.

As noted above in subsection **2.3.3**, wave transits of polarizing beam splitters are very similar to those of calcite polarizers. ΣI is similarly conserved and the appropriate path assignment for an energy quantum on the incident wave is similarly deterministically mandated by the orientation (and arc span) of that objectively real incident state. By **RULE 2** for polarizer emission states, the output states for both types of polarizers emerge with orientations of random members of vertical and horizontal linear polarization ensembles.

There are however important fundamental, subtle differences between the output states of those two types of polarization-based beamsplitters. The randomly oriented output states of the calcite polarizer emerge at physically separated locations on the exit face of the calcite. Those output states are represented as $\mathbf{\Phi}_{2a}(0°_\alpha)$ and $\mathbf{\Phi}_{3a}(90°_\beta)$ in Eq's. (20.2) and (21.2), respectively. Conversely, the output states for the polarizing beam splitter, as in subsection **2.3.3**, are emitted from a local region in the PBS dielectric contiguous to the local region where the incident state is split into planar waves. For the PBS those corresponding output states are represented as $\mathbf{\Phi}_4(0°_\alpha)$ and $\mathbf{\Phi}_5(90°_\alpha)$ in Eq's. (22.2) and (23b.2), respectively.

For the calcite polarizer, the random orientations are mutually non-correlated because of the physical separation of the emission loci. That non-correlation of output orientations for the calcite polarizer is appropriately specified by employing differing subscripts α and β where in general α≠β. Conversely, for the PBS the random orientations are mutually locally correlated because of the physical contiguity of polarizer emission and incident wave splitting in the dielectric. That local correlation of orientations for the PBS is appropriately represented by specifying the same α subscript on both output states. These differences between calcite and PBS outputs have important consequences in our subsequent analyses of loops incorporating these two types of polarizing beamsplitter devices.

When considering the wave input and output processes for a single channel of both types of beamsplitter polarizers, calcite and PBS, as well as for a single channel plate polarizer, the statistical outcomes are independent of the particular polarizer type. CI and LR are in agreement on this point.

However, we are reminded that CI photons emerging from a first polarizer with a 0° oriented axis are all representable by the same 0° definite linear polarization state. When a subsequent, subsequent polarizer is oriented at θ, statistically the transmission proportion of those identically represented photons is given by $\cos^2 \theta$. That outcome is consistent with the treatment of the photon as a probabilistic entity.

Conversely, the LR analysis of these results is that the CI definite linear polarization "state" is not a photon state but is more properly represented as an ensemble distribution of objectively locally real LR states. Each photon emitted by that first polarizer is a random LR member of that ensemble with a unique orientation and a fully deterministic outcome of being transmitted when encountering a subsequent, second polarizer oriented at some specified axial orientation θ.

Finally, we parenthetically note here that the atomic structure of polarizers literally "channels" LR waves onto a physically narrow path within the polarizer by transversely condensing those waves to propagate in a planar form. It is then seen as fortuitously prescient that two-axis polarizers such calcite and polarizing beamsplitters are commonly referred to as two-channel devices and similarly that single axis plate polarizers are commonly referred to as single-channel devices.

Appropriately, those two-channel and single channel appellations should be reserved for polarizers and not for dual output devices such as non-polarizing beamsplitters which do not similarly channel incident waves onto physically narrow paths. Through the arc condensation process, those channels play a critical role in deterministically mandating the assignment of an energy quantum onto a particular path within the polarizer.

3. Correlated Photons

3.1. Review of the LR Representation for Correlated Photons

Perhaps the greatest apparent impediment to the formulation of a viable locally real representation of quantum mechanics is the generally perceived exclusion of "locally real hidden variable theories" (LHVT's) based upon results of performed experiments for correlated states assessed in conjunction with Bell's inequality. [2-4]

In that regard, the particular LR representation of local realism ref. [1] derived from first principles of the underlying quantum formalism is shown to predict correlation measurements in agreement with that of CI and with results of performed Bell experiments despite that representation being an LHVT. That conundrum is addressed here.

In this subsection we briefly review the ref. [1] locally real treatment of correlated photons. Most notably for correlated pairs of photons such as from an atomic emission process (as well as for correlated pairs of particles) there is a naturally occurring asymmetry of the wave structures of the pair members.

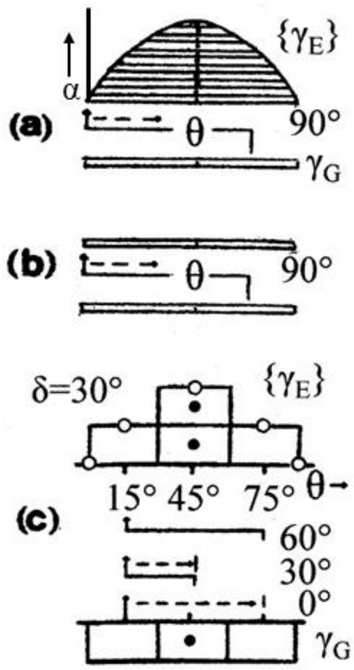

Fig. 5 (a-c): Bell measurement procedures showing photon arc spans and relative θ rotation of analyzers preceding the detectors: (a) for a correlated generator photon γ_G and a random member γ_E (a row) designated by α of the numerically partitioned correlated photon emission ensemble $\{\gamma_E\}$. The ensemble $\{\gamma_E\}$ member distribution is defined by the sin 2θ distribution envelope. (b) for a pair of identical photons. (c) for the alternative of an angularly partitioned correlated photon ensemble $\{\gamma_E\}$, which includes only two members for a 30° partition.

For photons, this asymmetry is manifested by one pair member, the "generator" photon, having a "full complement" Δ_G=90° arc span while the "emission" photon it produces has an arc span Δ_E≤90° that ranges from 0 to 90°. The particular Δ_E value for any correlated photon pair is that of a random member of a well-defined "emission ensemble" of correlated photons. The average arc span of the emission ensemble members is approximately 2/3 of the 90° arc span and the emission photons are characterized as having a "partial complement" arc span. Additionally, the generator photon and the emission photon arcs of every pair of correlated photons have aligned bisectors and those arcs can be conveniently represented on a common-orientation reference frame as in Fig. 5(a).

Fig. 5 (a) illustrates the 90° arc span of the generator member photon γ_G of a polarization correlated photon pair. The other member is an "emission photon" γ_E that is a random member of a finite-member correlated photon emission ensemble $\{\gamma_E\}$. The figure depicts N=11 members (rows) in that ensemble individually identified by α=1→11 where α=1 for the bottom row member. As $N\rightarrow\infty$ the envelope of $\{\gamma_E\}$ converges to sin 2θ with a distribution of arc spans ranging from 0° to 90°.

The arc spans of the individual $\alpha=1\rightarrow N$ members are given by the N-dependent equation

$$\Delta_{E\alpha}=90° - \sin^{-1} [(\alpha-1)/(N-1)] \tag{1.3}$$

where, for Fig. 5(a), N=11. Appropriately then, an ensemble such as that depicted in Fig. 5(a) is further identified as a "numerically partitioned correlated photon emission ensemble." In this case the equation Eq. (1.3) defines the unique arc span variable of each α member. This identification is in analogy to numerically partitioned polarization emission ensembles such as that depicted in Fig. 2 where an N-dependent equation Eq. (14.2) defines the unique orientation variable of each α member where all members have 90° arc spans.

To compute the correlation relationship, a coordinate frame of reference can be set up as illustrated in Fig. 5 (a). The solid arrow shows the points of coincident samplings on γ_G and $\{\gamma_E\}$ when the respective detectors in a Bell experiment are preceded by analyzers (polarizers) relatively rotated by θ. The dashed line shows the effective scanning of that sampling process as a large number of coincident samplings are acquired. Because of the partial complement arc span of the emission member, a "correlated" pair of generator and emission photons results in the characteristic quantum mechanical joint polarizer sampling of $\cos^2\theta$. This result more precisely reduces to ½ $\cos^2\theta$ because of null samplings beyond the sin 2θ envelope.

In contrast, as shown in Fig. 5 (b), a pair of ordinary full complement photons extracted from a single coherent wave occupied by two energy quanta are fully symmetric and identical in every sense including a common bisector orientation and a common full complement arc span. When such pairs are subjected to a Bell-experiment joint polarizer sampling the result is a linear ½(1-2θ/90°) over 0° to 90°. These symmetric photons are certainly also "correlated" but are clearly distinguishable from the asymmetric generator-emission pair which exhibit a (½)$\cos^2\theta$ joint polarizer sampling.

Fig. 5 (c) is a highly simplified alternative representation relative to the Fig. 5 (a) numerically partitioned ensemble $\{\gamma_E\}$ and its associated generator photon γ_G. In Fig. 5 (a) the multiplicity of Δ_E wave arcs approximates the actual infinite $\{\gamma_E\}$ ensemble members whereas in Fig. 5 (c) the model partitions those arcs into 30° "δ wave packets" purely as a mathematical intermediary for the purposes of implementing a finite number of Bell samplings. That partitioning reduces the actual infinite-member emission ensemble $\{\gamma_E\}$ to a mere two members, a γ_{E1} comprised of a single δ wave packet and a γ_{E2} comprised of three δ wave packets, the same as that of the γ_G. Notably, the five circles on the Fig. 5 (c) $\{\gamma_E\}$ constitute an exact fit to the sin2θ envelope of the infinite-member limit for Fig. 5 (a) $\{\gamma_E\}$.

The depiction of $\{\gamma_E\}$in Fig. 5 (c), in contrast to the numerically partitioned Fig. 5(a) depiction of $\{\gamma_E\}$constitutes an angularly partitioned correlated photon emission ensemble. Accordingly, $\{\gamma_E\}$ in Fig. 5(c) is appropriately further identified as an "angularly partitioned" correlated photon emission ensemble. This identification is in analogy to angularly partitioned polarization emission ensembles such as that depicted in Fig. 3.

The evaluation of joint transmission is totally trivial by inspection. With respect to the Fig. 5(c) frame, when the polarizers are not relatively rotated, $\theta=0°$ and there are 4 joint transmissions of γ_G with photons in $\{\gamma_E\}$. When $\theta=30°$, there are 3 joint transmissions. For $\theta=60°$, there is 1 joint transmission. For $\theta=90°$ and beyond (not depicted), there are 0 joint transmissions. After normalization, these results give exact agreement with $\frac{1}{2}\cos^2\theta$. This is entirely a locally determined correlation that persists as γ_G and γ_E move apart. There is no non-local phenomenon of entanglement invoked in the process of achieving the correlation.

Importantly, straightforward integrations computing joint transmissions for the Bell measurements associated with the Fig. 5 (a) continuous distribution when $N\to\infty$ yield the same conclusion that there is no non-local phenomenon of entanglement invoked in the LR representation. [1]

From the perspective of LR, asymmetric pairs as in Fig. 5(a) exhibit mathematical correlation levels that are directly attributable to their respective objectively real structures. Conversely, because of the explicit CI exclusion of objectively real structures, entities that are identified as being correlated by an interaction process necessarily are interpreted as exhibiting the non-local phenomenon of entanglement upon being measured.

Finally, it is important to review the above results and their relationship to Bell's inequality.[2] A consequence of the asymmetry of the generator-emission pairs is that correlated emission members exhibit the property of "enhancement" when measured.[1] and [5]

In the context of photons, enhancement means that the transmission of an objectively real fully specified photon through a randomly oriented polarizer is enhanced by transmitting that photon through a second, specified polarizer. A full complement photon, such as a generator photon, has a 50% mathematical probability of being transmitted through a randomly oriented polarizer whereas for an average correlated emission photon that mathematical probability drops to ~(2/3)50%.

However, if a correlated emission photon is transmitted through a polarizer, that correlated emission photon emerges as a full complement $\Delta=90°$ arc span photon with a subsequent mathematical transmission probability through a randomly oriented polarizer of 50%. As a result, transmission of the correlated emission photon member of a correlated pair through a polarizer enhances that photon's mathematical transmission probability through a subsequent randomly oriented polarizer. (A similar analysis for particles yields a corresponding outcome. [1])

Clauser and Horne [5] deduced a general rule that locally real hidden variable theories that exhibit enhancement are not subject to Bell's inequality. [2] However, this exclusion was not considered to be a viable loophole for LHVT's because the property of enhancement was conjectured to be an implausible physical property, i.e. transmitting a photon through a polarizer plausibly should not increase its transmission probability through a subsequent, randomly oriented polarizer. As a counterexample to this conjecture, enhancement does arise as a natural and plausible physical property of LR. This does not constitute a conundrum with regard to Bell's inequality and LR since we can conclude that it is the conjecture itself that is incorrect. [1]

Because of the flawed conjecture that all physically viable LHVT's had the property of non-enhancement, the reported Bell experiments in conjunction with Bell's Theorem have effectively led to the general perception that the entire class of LHVT's has been disproved. A consequent corollary to this perception is that pairs of photons (or particles) that exhibit the characteristic quantum correlation are automatically inferred to be non-locally entangled. "The perception of entanglement is a consequence of the subtlety of enhancement." [1]

3.2. A Critical Analysis of the CI Representation for Correlated Photons

Historically, the CI treatment of correlated photon states has profoundly impacted the treatment of quantum phenomena. We further examine that CI treatment of correlated photons here in part because of that impact and in part because, from the perspective of LR, the CI treatment improperly applies the standard linear polarization states.

In this report we have deduced particular locally real states consistent with LR in replacement of the ubiquitous CI linear polarization state. From the LR analysis of correlated photons, distinctively different locally real states have been deduced. For a correlated photon pair, denoted as γ_1 and γ_2, CI postulates that when γ_1 is successfully measured by transmission through the 1st Bell polarizer oriented at 0°, the γ_2 mate is instantly in a definite correlated state relative to that of γ_1 constrained by angular momentum conservation. In the positivist-based CI that definite correlated state is implicitly equivalent to a definite 0° polarization state that should be transmitted by the 2nd Bell polarizer at θ with the characteristic $\cos^2 \theta$ distribution associated with polarizer emission.

From the perspective of LR that γ_2 mate of the correlated pair is not in a state generated from a definite polarization state. There is no polarizer present from which a definite polarization state would be generated. LR shows that it is the objectively real planar state photon propagating within a polarizer and transversely confined at the orientation of the polarizer axis that is responsible for generating the ensemble associated with a definite polarization state. However, that planar state is absent in the correlated pair. LR self-consistently shows that it is the correlated pair photon with a full complement 90° arc span and designated as the generator photon γ_G, i.e. γ_1, that generates a "correlated photon emission ensemble" $\{\gamma_E\}$. From that ensemble $\{\gamma_E\}$ a single random member γ_E, i.e. γ_2, is emitted without incurring the phenomenon of non-local entanglement. [1]

LR shows that it is incorrect for CI to interpret that γ_2 of the correlated pair is in the same "definite linear polarization state" as γ_G, i.e. γ_1. The member γ_E, i.e. γ_2, must conserve angular momentum relative to γ_G because the pair arises in free space. This conservation is satisfied in LR by the associated correlated photon emission ensemble $\{\gamma_E\}$. The emission ensemble is shown to be generated from the full 90° arc span of the "generator" photon. [1] Significantly, all members of that $\{\gamma_E\}$ emission ensemble inherently have the same orientation, ensuring conservation of angular momentum with respect to the generator photon. Despite the differences in the definite linear polarization ensemble $\{\gamma_e\}$ and the correlated photon emission ensemble $\{\gamma_E\}$ with its spectrum of arc spans, we still get a joint transmission distribution with the polarizer of the 2nd

Bell detector not distinguishable from that predicted by CI for Bell experiments. Ultimately, since the mutual alignment of the generator photon γ_G and the $\{\gamma_E\}$ ensemble occurs locally at the atomic system, the correlation is local.

In contrast, from the perspective of LR, polarizer emitted states do not conserve angular momentum relative to the planar photon that generates those states because the polarizer emission process includes the massive polarizer itself. The output states of the polarizer exhibit a spectrum of orientations relative to the planar generator photon. That spectrum is incompatible with the constraint of angular momentum conservation for correlated pair members. However, that constraint is satisfied by the LR $\{\gamma_E\}$ in which all members have the same orientation as γ_G.

4. Photon Transits of Conventional Loops

4.1. Photon Wave Transits of a Mach-Zehnder Loop Equipped with Non-polarizing Beam Splitters

Mathematically, the CI and the LR equations relating to photon transits of the Fig. 6 Mach-Zehnder loop equipped with non-polarizing beam splitters are fundamentally equivalent. The essential difference resides with the physical interpretations of the represented quantities in those equations.

For LR the waves on the two legs of the loop constitute real physical entities split from the real physical entity of a loop-incident wave. $\sqrt{2}/2$ amplitude coefficients on those split wave entities arising from a 50:50 beamsplitter constitute real physical amplitude magnitudes of the waves on the two legs where the incident photon wave amplitude magnitude is normalized to unity strictly as a calculational convenience. A complete accounting of the photon loop transits must treat the two cases of incident photon wave energy quantum transfer: (1) onto the clockwise loop path and (2) onto the counter-clockwise loop path. In each case an objectively real empty wave propagates on the other path. There are four transition sequences of real LR wave states progressing from the incident $\mathbf{\Phi}_1(\theta)_+$ on path 1 to the output states on joint path 4,8 which combines two of those sequences and joint path 5,9 which combines the other two sequences. Aside from the assignment of occupancy or non-occupancy, i.e. the presence or absence of a + subscript, the sequences below are fully deterministic with regard to the wave amplitudes. In this exercise we assign occupancy to the clockwise paths without loss of generality.

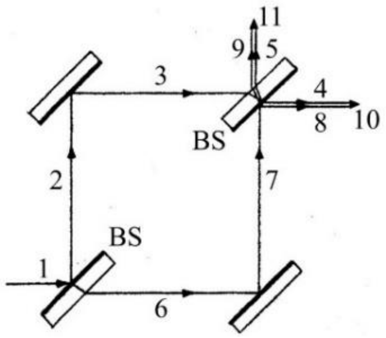

Fig. 6: Transit of a photon wave through a Mach-Zehnder loop equipped with non-polarizing 50:50 beamsplitters.

The 1st set of sequences

$$\mathbf{\Phi}_1(\theta)_+=\xi 1\ \mathbf{r}(\theta)_+\rightarrow_{\text{BS-r}}$$

$$\mathbf{\Phi}_2(\theta)_+= -\xi(\sqrt{2}/2)\mathbf{r}(\theta)_+\rightarrow_{\text{mir}}$$

$$\mathbf{\Phi}_3(\theta)_+=\xi(\sqrt{2}/2)\mathbf{r}(\theta)_+\rightarrow_{\text{BS-r}}$$

$$\mathbf{\Phi}_5(\theta)=\xi(1/2)\mathbf{r}(\theta) \tag{1.4}$$

and

$$\mathbf{\Phi}_1(\theta)_+=\xi 1\ \mathbf{r}(\theta)_+\rightarrow_{\text{BS-t}}$$

$$\mathbf{\Phi}_6(\theta)=\xi(\sqrt{2}/2)\mathbf{r}(\theta)\rightarrow_{\text{mir}}$$

$$\mathbf{\Phi}_7(\theta)= -\xi(\sqrt{2}/2)\mathbf{r}(\theta)\rightarrow_{\text{BS-t}}$$

$$\mathbf{\Phi}_9(\theta)= -\xi(1/2)\mathbf{r}(\theta). \tag{2.4}$$

both conclude with LR wave states on the emergent joint path 5,9. The subscripts denote the particular interaction at each sequence transition. The joint paths 5,9 are physically contiguous and can be redefined as path 11. The resident states are summed giving

$$[\mathbf{\Phi}_5(\theta)=\xi(1/2)\mathbf{r}(\theta)_+] + [\mathbf{\Phi}_9(\theta)= -\xi(1/2)\mathbf{r}(\theta)] \rightarrow_{\text{sum}}$$

$$\mathbf{\Phi}_{11}(\theta) =\xi 0\mathbf{r}(\theta). \tag{3.4}$$

Accordingly, the 11 path has a zero-magnitude amplitude and cannot sustain the energy quantum that reaches the 2nd beam splitter whether by path 3 as indicated above or by path 7 which is not indicated above.

However, the 2nd set of sequences deterministically results in a unit magnitude amplitude on the emergent path 10.

$$\mathbf{\Phi}_1(\theta)_+=\xi 1\ \mathbf{r}(\theta)_+\rightarrow_{\text{BS-r}}$$

$$\mathbf{\Phi}_2(\theta)_+ = -\xi(\sqrt{2}/2)\mathbf{r}(\theta)_+ \rightarrow_{\mathrm{mir}}$$

$$\mathbf{\Phi}_3(\theta)_+ = \xi(\sqrt{2}/2)\mathbf{r}(\theta)_+ \rightarrow_{\mathrm{BS\text{-}t}}$$

$$\mathbf{\Phi}_4(\theta)_+ = \xi(1/2)\mathbf{r}(\theta)_+ \tag{4a.4}$$

and

$$\mathbf{\Phi}_1(\theta)_+ = \xi 1\, \mathbf{r}(\theta)_+ \rightarrow_{\mathrm{BS\text{-}t}}$$

$$\mathbf{\Phi}_6(\theta) = \xi(\sqrt{2}/2)\mathbf{r}(\theta) \rightarrow_{\mathrm{mir}}$$

$$\mathbf{\Phi}_7(\theta) = -\xi(\sqrt{2}/2)\mathbf{r}(\theta) \rightarrow_{\mathrm{BS\text{-}r}}$$

$$\mathbf{\Phi}_8(\theta) = \xi(1/2)\mathbf{r}(\theta). \tag{4b.4}$$

Note that the two phase flips at the mirrors could have been ignored in Eq.'s (4a.4) and (4b.4) because the relative phase on the two legs is not altered in that process.

The joint paths 4,8 are physically contiguous and can be redefined as path 10. The states can be summed giving

$$[\mathbf{\Phi}_4(\theta)_+ = \xi(1/2)\mathbf{r}(\theta)_+] + [\mathbf{\Phi}_8(\theta) = \xi(1/2)\mathbf{r}(\theta)] \rightarrow_{\mathrm{sum}}$$

$$\mathbf{\Phi}_{10}(\theta)_+ = \xi 1 \mathbf{r}(\theta)_+. \tag{5.4}$$

It may be appreciated that if the energy quantum were instead on the counterclockwise paths the energy quantum would still transition to path 4,8=10.

For the positivist-based CI, the waves on the respective two legs are necessarily probabilistic, non-real, entities because the existence of a physically real empty wave on one of the legs is not directly susceptible to experimental confirmation. Consistent with this probabilistic interpretation, the physical separation of the two legs further requires that the entities on the two legs constitute a state of non-local superposition of probabilistic waves extracted from the single loop-incident wave.

The corresponding CI representation of the Fig. 6 loop transits is given below where the ket subscripts identify the respective loop paths.

$$1|x\rangle_1 \rightarrow_{\mathrm{mir}}$$

$$(-\sqrt{2}/2)|y\rangle_2 + (\sqrt{2}/2)|x\rangle_6 \rightarrow_{\mathrm{mir}}$$

$$(\sqrt{2}/2)|x\rangle_3 + (-\sqrt{2}/2)|y\rangle_7 \tag{6.4}$$

The path 2 and 6 terms explicitly represent a non-local superposition state of the loop-incident state $1|x\rangle_1$ as it transits the first half of the loop legs. Similarly, the path 3 and 7 terms represent that non-local superposition state as it continues onto the second half of the loop legs after respective phase flipping reflections from the mirrors.

When the Eq. (1.4) non-local superposition state is incident on the second beamsplitter, components of that state are projected onto the dual output paths, 10 and 11, giving respectively

$$[(\sqrt{2}/2)\,(\sqrt{2}/2) + (\sqrt{2}/2)\,(\sqrt{2}/2)]|x\rangle_{10} = 1|x\rangle_{10} \tag{7.4}$$

and

$$[(\sqrt{2}/2)\,(\sqrt{2}/2) + (\sqrt{2}/2)\,(-\sqrt{2}/2)]|y\rangle_{11} = 0|y\rangle_{11}. \tag{8.4}$$

The summed terms on Eq's. (7.4) and (8.4) are local superpositions of Eq. (1.4) projection components and respectively constitute the output states $1|x\rangle_{10}$ and $0|y\rangle_{11}$. The unit coefficient of $|x\rangle_{10}$ confirms for CI that the incident photon, which had been in non-local superposition on the loop, emerges on the path 10 output of the second beamsplitter.

An important point to be stressed for CI is that a successful measurement of the energy quantum associated with a photon on one of the legs immediately and non-locally elevates the coefficient on that leg to unity consistent with the incident wave photon and collapses (extinguishes) the $\sqrt{2}/2$ coefficient on the probabilistic wave state on the other leg to conserve probability. That non-local process is required by CI which treats the wave-like amplitude and the particle-like energy quantum as different aspects of the same entity.

Conversely for LR, when a detector inserted into one leg of the loop intercepts an occupied wave, the resultant detector measurement is physically indistinguishable from that of the detector intercepting either the loop-incident (occupied) photon wave or the loop-emergent (occupied) photon wave. Notably, the indistinguishability of detector measurements occurs despite the wave amplitude magnitudes in the two cases being respectively $\sqrt{2}/2$ and 1.

4.2. Photon Transits of a Loop Comprised of Contiguous Calcite Polarizers

We analyze here the photon transit of the contiguous calcite loop depicted in Fig. 7 for LR. That loop consists of a pair of contiguous, oppositely oriented calcite polarizers. We examine the transit of an amplitude oriented in the range from −45° to +45° without loss of generality since analysis with the orthogonal range from +45° to +135°, is straightforward from symmetry considerations. Over that −45° to +45° range we can conveniently specify a particular orientation as $0°_\alpha$.

The (unit modulus) amplitude incident on path 1 is

$$\mathbf{\Phi}_1(0°_\alpha)_+ = \xi\, \mathbf{r}(0°_\alpha)_+. \tag{9.4}$$

Continuing onto path 2, the amplitude

$$\mathbf{\Phi}_{\delta 2}(0°)_+ = \xi \cos 0°_\alpha\, \mathbf{r}_\delta(0°)_+ \tag{10.4}$$

is a δ-form planar wave because it is propagating inside a polarized medium. $\mathbf{\Phi}_{\delta 2}$ retains the energy quantum that had been on $\mathbf{\Phi}_1(0°_\alpha)_+$ because the transverse arc for that $0°_\alpha$ bisector orientation intersects the 0° polarization axis of calcite 10.

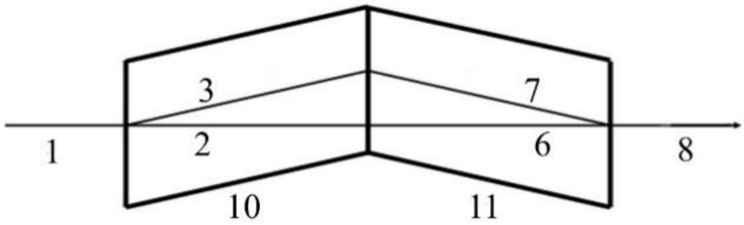

Fig. 7 A loop comprised of contiguous calcite crystals. An input photon expressed as a locally real state is deterministically replicated at the loop output without non-local superposition as a result of local correlation that occurs at the loop input.

For path 6 the amplitude

$$\mathbf{\Phi}_{\delta 6}(0°)_{+}=\mathbf{\Phi}_{\delta 2}(0°)_{+} \tag{11.4}$$

resulting in

$$\mathbf{\Phi}_{\delta 6}(0°)_{+}= \xi \cos 0°_{\alpha}\, \mathbf{r}_{\delta}(0°)_{+} \tag{12.4}$$

since calcites 10 and 11 are contiguous and there is no amplitude transition in the passage from the vertical 0° polarization channel on calcite 10 to that on calcite 11.

The path 3 amplitude

$$\mathbf{\Phi}_{\delta 3}(90°)= \xi \sin 0°_{\alpha}\, \mathbf{r}_{\delta}(90°) \tag{13.4}$$

is the complementary horizontal axis projection of the incident amplitude. $\mathbf{\Phi}_{\delta 3}$ is an empty wave because of the orientation constraint $-45°<0°_{\alpha}<+45°$ on $0°_{\alpha}$. In analogy to the $\mathbf{\Phi}_{\delta 2}(0°)_{+}$, $\mathbf{\Phi}_{\delta 6}(0°)_{+}$ equivalence the amplitude on path 7 is

$$\mathbf{\Phi}_{\delta 7}(90°)=\xi \sin 0°_{\alpha}\, \mathbf{r}_{\delta}(90°). \tag{14.4}$$

With in-phase conditions present for the two orthogonal amplitudes converging at the output face of calcite 11, the vector sum of

$$\begin{aligned}\mathbf{\Phi}_{\delta 6}(0°)_{+}+ \mathbf{\Phi}_{\delta 7}(90°)&=\xi\, [\cos 0°_{\alpha}\, \mathbf{r}_{\delta}(0°)_{+}+ \sin 0°_{\alpha}\, \mathbf{r}_{\delta}(90°)]\\ &=\xi\, \mathbf{r}(0°_{\alpha})_{+}\\ &=\mathbf{\Phi}_{8}(0°_{\alpha})_{+}\end{aligned} \tag{15.4}$$

consistent with **RULE 2** of polarizer emission.

This conjuncture at the calcite 11 exit face results in a loop output wave identical to the input wave consistent with the unitary property of the calcite loop required by the underlying quantum formalism. However, this LR result does not impose the non-local superposition necessitated when the loop transit is represented by CI.

Because the loop transits are completely deterministic, the state of each objectively real input state at any θ within the range $-45°<\theta<+45°$ is exactly replicated at output. Accordingly, symbolically Fig. 8 is a vector diagram of the loop input states as well as the loop output states employing the Fig. 3 ensemble.

For example, the "A" input state of the Fig. 8 LR polarization ensemble at −30° is replicated as a −30° output state. This process continues for each input state in the continuum limit as δ→0°, trivially replicating the entire input set of states at the loop output. When the input set happens to have the characteristic distribution of a linear polarization ensemble, the output distribution under one-for-one replication will trivially also have that characteristic distribution.

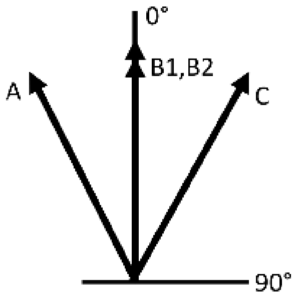

Fig. 8 A symbolic vector diagram of a definite vertical (0°) linear polarization ensemble depicting the four locally real states of the angularly partitioned Fig. 3 ensemble $\{\gamma_e\}$.

Moreover, under one-for-one replication, any input distribution would be replicated because of the local correlation that occurs as each photon enters the loop. No non-local superposition is present.

In contrast, CI treats the definite 0° linearly polarized input state as a probabilistic entity that does not admit any objectively real structure to that input state. That treatment necessarily imposes non-local superposition in the loop transit process. See subsection **4.5.** below.

Ultimately, the LR and the CI treatments both yield statistically indistinguishable output results but with the CI treatment necessarily imposing non-local superposition.

4.3. Photon Transits of a Loop Comprised of Non-contiguous Calcite Polarizers

Photon transits of a non-contiguous opposed calcite loop present an interesting contrast to that of the contiguous opposed calcite loop considered above. For this Fig. 9 non-contiguous variant a conventional definite CI polarization state at the input of the loop apparently results in an identical definite CI polarization state at the output of the loop. From the perspective of LR, that state replication is questionable.

From subsection **3.2.**, Eq's. (10.4) and (13.4) for a contiguous calcite loop, we see that the respective states on paths 2 and 3 have maintained a local correlation acquired as the incident state on path 1 entered calcite 10. That condition is similarly applicable in the present case of a non-contiguous calcite loop. However, for that non-contiguous calcite loop when the states on paths 2 and 3 reach the exit face of calcite 10, two spatially separated, mutually uncorrelated random polarizer emission states are generated respectively onto paths 2a and 3a. As a result, the original local correlation that was present on the path 2 and path 3 states should no longer be present because of the uncorrelated emissions that occurred at the exit face of calcite 10.

For instructional purposes in this analysis, without loss of generality, we consider a CI diagonal definite linear polarization state input on path 1 of Fig. 9. In LR that diagonally polarized input state is represented by $\mathbf{\Phi}_1(45°_\alpha)_+$ where α specifies some random member of the $45°_\alpha$ diagonally oriented linear polarization ensemble. A large number of those objectively real random members would trivially yield the probabilistic distribution associated with a CI diagonal definite linear polarization state if the calcite crystals were instead contiguous.

For the Fig. 9 analysis the LR input state is

$$\mathbf{\Phi}_1(45°_\alpha)_+ = \xi\, \mathbf{r}(45°_\alpha)_+ \tag{16.4}$$

where, as usual, ξ represents the normalized longitudinal wave function.

When $\mathbf{\Phi}_1(45°_\alpha)_+$ is incident on calcite 10, the state is split into the two planar wave states

$$\mathbf{\Phi}_{\delta 2}(0°)_+ = \xi \cos(45°_\alpha)\, \mathbf{r}_\delta(0°)_+ \tag{17a.4}$$

and

$$\mathbf{\Phi}_{\delta 3}(90°) = \xi \sin(45°_\alpha)\, \mathbf{r}_\delta(90°). \tag{17b.4}$$

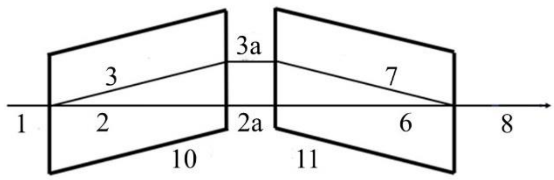

Fig. 9: A loop comprised of non-contiguous calcite crystals. An input photon expressed as a locally real state is statistically replicated at the loop output.

In this representation of the two planar wave states, Eq.'s (17a.4) and (17b.4), we have again imposed an initial condition on the orientation of the incident photon for instructional purposes and without loss of generality. In this initial condition the random ensemble member α is associated with a member that has its arc bisector orientation θ confined to $0°<\theta<+45°$ (as opposed to $+45°<\theta<+90°$). As a result, the energy quantum residing on $\mathbf{\Phi}_1(45°_\alpha)_+$, is transferred to the vertically projected state component $\mathbf{\Phi}_{\delta 2}(0°)_+$ as indicated by the appended "+" subscript that is not appended to the horizontally projected state component $\mathbf{\Phi}_{\delta 3}(90°)$. This imposed condition allows us to progressively track the energy quantum as the wave states transit the loop but does not otherwise alter the wave states. $\mathbf{\Phi}_{\delta 2}(0°)_+$ is then identifiable as a photon or, equivalently, an occupied wave whereas $\mathbf{\Phi}_{\delta 3}(90°)$ is an empty wave.

At the exit face of calcite 10, the physically separated planar waves $\mathbf{\Phi}_{\delta 2}(0°)_+$ and $\mathbf{\Phi}_{\delta 3}(90°)$ respectively emit the states

$$\mathbf{\Phi}_{2a}(0°_\mu)_+ = \xi \cos(45°_\alpha)\, \mathbf{r}(0°_\mu)_+ \tag{18a.4}$$

and

$$\boldsymbol{\Phi}_{3a}(90°_\nu)= \xi \sin(45°_\alpha)\, \mathbf{r}(90°_\nu). \tag{18b.4}$$

Because of their physical separation, the μ and ν ensemble members emitted from the calcite 10 in Fig. 9 are mutually uncorrelated with respect to arc bisector orientations. (See analysis of Fig. 4(b) calcite beamsplitter outputs.)

When the uncorrelated $\boldsymbol{\Phi}_{2a}(0°_\mu)_+$ and $\boldsymbol{\Phi}_{3a}(90°_\nu)$ are incident on calcite 11 of Fig. 9, they respectively generate planar wave states

$$\boldsymbol{\Phi}_{\delta 6}(0°)_+= \xi \cos(45°_\alpha) \cos(0°_\mu)\, \mathbf{r}_\delta(0°)_+ \tag{19a.4}$$

and

$$\boldsymbol{\Phi}_{\delta 7}(90°)= \xi \sin(45°_\alpha) \sin(90°_\nu)\, \mathbf{r}_\delta(90°), \tag{19b.4}$$

that propagate in calcite 11. At the exit face of calcite 11 those planar wave states vectorially combine to produce

$$\boldsymbol{\Phi}_{\delta 6}(0°)_+ + \boldsymbol{\Phi}_{\delta 7}(90°)=$$

$$\xi[\cos(45°_\alpha)\cos(0°_\mu)\mathbf{r}(0°)+\sin(45°_\alpha)\sin(90°_\nu)\mathbf{r}(90°)]_+ \tag{20a.4}$$

In those infrequent particular instances, in which μ=ν, $\cos(0°_\mu)=\sin(90°_\nu)$, and Eq. (20a.4) reduces to the compact form

$$\begin{aligned} &\boldsymbol{\Phi}_{\delta 6}(0°)_+ + \boldsymbol{\Phi}_{\delta 7}(90°) \\ &= \cos(0°_\mu)\, \xi\, \mathbf{r}(45°_\alpha) \\ &=\boldsymbol{\Phi}_8(45°_\alpha)_+ \\ &= \cos(0°_\mu)\, \boldsymbol{\Phi}_1(45°_\alpha)_+. \end{aligned} \tag{20b.4}$$

For those infrequent instances, the output state $\boldsymbol{\Phi}_8(45°_\alpha)_+$ would, most importantly, replicate the orientation of the input state $\boldsymbol{\Phi}_1(45°_\alpha)_+$. Of secondary interest, the output amplitude $\boldsymbol{\Phi}_8(45°_\alpha)_+$ is reduced by a projection factor such as $\cos(0°_\mu)$ relative to the input amplitude $\boldsymbol{\Phi}_1(45°_\alpha)_+$.

However, because of the typical μ≠ν non-correlation, a particular loop output state of Eq. (20a.4) does not generally replicate the orientation of an input $\boldsymbol{\Phi}_1(45°_\alpha)_+$ state as it would have if the calcites were contiguous. Because of that general non-replication for individual input states, an input comprised of an entire linear polarization ensemble of those individual states may produce an output distribution that is measurably distinct from that of the ubiquitous linear polarization state predicted by CI for the non-contiguous calcite loop. Accordingly, the resultant output distribution must be assessed.

For our purposes here a sufficient assessment can most succinctly and instructively be conducted using an N=4 member angularly partitioned polarization ensemble. That ensemble is similar to that of Fig. 3 where angular increments are still partitioned into 30° intervals but where the $\{\gamma_e\}$ ensemble is centered at 45° instead of 0° in order to properly represent a diagonally polarized input ensemble. The statistically complete evaluation of all possible combinations of α, μ and ν requires the computation of only 64 loop transits from Eq. (20a.4).

Fig. 10 depicts the corresponding vector representation of that diagonally polarized ensemble with member states at 15°, 45°, 45° and 75°. The α member indices 1, 2, 3, and 4 may be assigned respectively to the vector states C, B2, B1, and A. The Fig. 6 vertically polarized ensemble with member states at −30°, 0°, 0° and +30° and the Fig. 8 horizontally polarized ensemble with member states at +60°, +90°, +90° and +120° are also similarly used in the simulation respectively for quantities having μ and ν indices. The computation involves 4^3=64 evaluations of Eq. (20a.4) but the symmetry of input A and C states and the redundancy of B1 and B2 states effectively reduce the mathematically unique computations of Eq. (20a.4) to 16. The states on the two legs of the loop each acquire a deterministic set of amplitude coefficients as they enter the first calcite polarizer. As those respective states exit that first polarizer the respective states are uncorrelated in orientation but they still respectively retain the deterministic set of amplitude coefficients acquired at that first calcite polarizer. When those states enter the second calcite polarizer they acquire a second set of amplitude coefficients, each having multiple values statistically accounting for all possible orientation combinations of the uncorrelated states on both legs. The computations demonstrate most notably that, despite the non-correlation of the respective states on the two legs, the orientations of the output states from the loop average precisely to the same orientations 15°, 45°, 45° and 75° otherwise associated with the four μ=ν combinations. Those averaged output states are depicted in the Fig. 11 symbolic vector diagram.

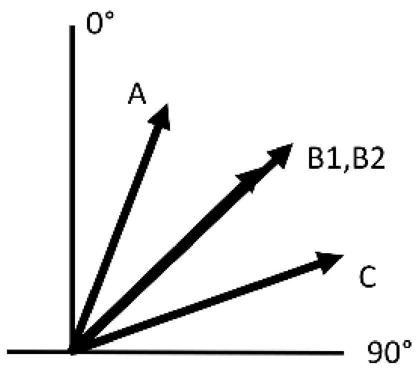

Fig. 10: A symbolic vector diagram of the four locally real states in a 30° angularly partitioned linear polarization ensemble $\{\gamma_e\}$. The ensemble is diagonally polarized.

There are symmetrical dispersions of resultant orientations about each of those averaged orientations because of the relative non-correlation of state orientations introduced as the states exit the first polarizer. These dispersions, expressed as standard deviations, are ~2.8° at 45° and ~1.4° at 15° and 75°.

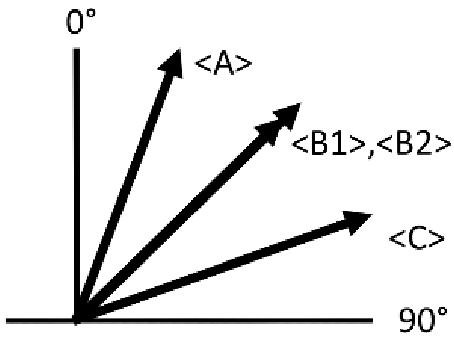

Fig. 11: A symbolic vector diagram depicting the four locally real averaged states emerging from the Fig. 9 loop when the Fig. 10 states are input

The statistical replication of output state orientation relative to input state orientation is explicitly shown here for the particular case of a coarse 30° angularly partitioned ensemble. However, that replication is readily shown to persist for finer angularly partitioned ensembles.

As a result, the easily computed loop output example using a coarse 30° angularly partitioned ensemble provides a basis for generalizing that an infinitesimally fine angularly partitioned ensemble statistically replicates the distribution of a CI linear polarization state.

This analysis is significant because it shows that the Fig. 9 non-contiguous calcite loop results in statistical replication of the input definite "state" distribution despite the lack of local correlations that render the loop transit as a non-unitary process. This replication can be attributed to the global symmetry of the loop.

Then as a practical matter, an actual experiment, where real ensembles are infinitesimally angularly partitioned, is expected to yield a statistical output distribution that is substantially indistinguishable from a CI linearly polarization state distribution.

Finally, we note that transits of the LR states through a non-contiguous calcite loop do not invoke non-local superposition.

4.4. Photon Transits of a Mach-Zehnder Loop Equipped with Polarizing Beam Splitters

Fig. 12(a) illustrates a polarizing beam splitter Mach-Zehnder loop. The LR analysis of photon wave transit of this PBS M-Z loop is more involved than that of the Fig. 7 contiguous calcite loop but is nevertheless straightforward and fully consistent with previous analyses. In the LR analysis of the PBS M-Z loop, the wave's arc bisector orientation θ is first constrained to the range $-45°<\theta<+45°$ on the incident wave in the interests of providing an instructive example before considering the alternative range $+45°<\theta<+135°$. The input state

$$\mathbf{\Phi}_1(\theta)_+=\xi\,\mathbf{r}(\theta)_+. \tag{21.4}$$

Fig. 12 (b) is diagrammatic representation of the δ-form projections of $\mathbf{\Phi}_1(\theta)_+$ inside the dielectric layers of the PBS. The reflected amplitude is

$$\mathbf{\Phi}_{\delta 2}(0°)_+=\xi\cos(\theta)\,\mathbf{r}_\delta(0°)_+ \tag{22.4}$$

and since the current example has $-45°<\theta<+45°$ for the incident $\mathbf{\Phi}_1(\theta)_+$ the transmitted amplitude is

$$\mathbf{\Phi}_{\delta 3}(90°)=\xi\sin(\theta)\,\mathbf{r}_\delta(90°) \tag{23.4}$$

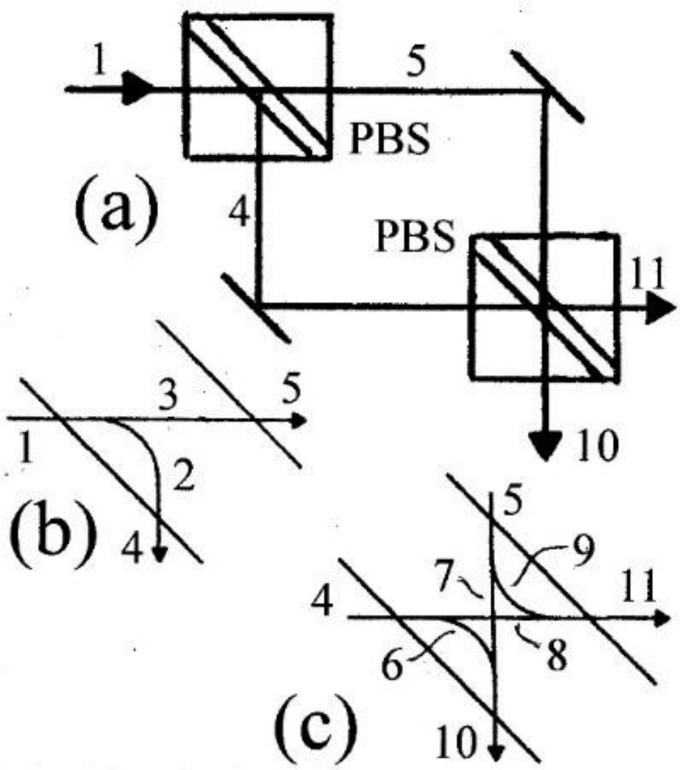

Fig. 12: Waves transiting a polarizing beam splitter Mach-Zehnder, PBS M-Z, loop. (a) the loop configuration, (b) and (c) detailed diagrammatic representations of waves transiting the respective PBS dielectric layers.

In a statistical emission process these amplitudes respectively produce

$$\mathbf{\Phi}_4(0°_\alpha)_+= \xi\cos(\theta)\,\mathbf{r}(0°_\alpha)_+ \tag{24a.4}$$

and

$$\mathbf{\Phi}_5(0°_\alpha+90°)=$$

$$\mathbf{\Phi}_5(90°_\alpha)=$$

$$\xi\sin(\theta)\,\mathbf{r}(90°_\alpha). \tag{24b.4}$$

See **2.3.3.** regarding local correlation in Eq.'s (24a.4) and (24b.4). This statistical emission process occurs at the output of a polarizer when an exit wave is unaccompanied by an orthogonal exiting wave.

After reflections at loop mirrors the respective projections of $\mathbf{\Phi}_4(0°_\alpha)_+$ and $\mathbf{\Phi}_5(90°_\alpha)$ inside the output PBS dielectric layers, Fig. 12(c), are the four δ-forms,

$$\mathbf{\Phi}_{\delta 6}(0°)_{+}=\xi\cos(\theta)\cos(0°_{\alpha})\mathbf{r}_{\delta}(0°)_{+}\,, \tag{25a.4}$$

$$\mathbf{\Phi}_{\delta 7}(90°)=\xi\sin(\theta)\sin(90°_{\alpha})\mathbf{r}_{\delta}(90°)$$

$$=\xi\sin(\theta)\cos(0°_{\alpha})\mathbf{r}_{\delta}(90°), \tag{25b.4}$$

$$\mathbf{\Phi}_{\delta 8}(0°)=\xi\cos(\theta)\sin(0°_{\alpha})\mathbf{r}_{\delta}(0°), \tag{26a.4}$$

and

$$\mathbf{\Phi}_{\delta 9}(90°)=\xi\sin(\theta)\sin(0°_{\alpha})\mathbf{r}_{\delta}(90°). \tag{26b.4}$$

The δ-form projections $\mathbf{\Phi}_{\delta 6}(0°)_{+}$ and $\mathbf{\Phi}_{\delta 7}(90°)$ sum vectorially giving a resultant on path 10, Fig.'s 12(a) and 12(c),

$$\mathbf{\Phi}_{\delta 6}(0°)_{+}+\mathbf{\Phi}_{\delta 7}(90°)$$

$$=\xi\cos(\theta)\cos(0°_{\alpha})\mathbf{r}_{\delta}(0°)_{+}+\xi\sin(\theta)\cos(0°_{\alpha})\mathbf{r}_{\delta}(90°)$$

$$=\xi\cos(0°_{\alpha})[\cos(\theta)\,\mathbf{r}_{\delta}(0°)_{+}+\sin(\theta)\mathbf{r}_{\delta}(90°)]$$

$$=\xi\cos(0°_{\alpha})\mathbf{r}(\theta)_{+}$$

$$=\mathbf{\Phi}_{10}(\theta)_{+}. \tag{27.4}$$

In Eq. (27.4) the resolution of the bracketed [ ] factor to $\mathbf{r}(\theta)_{+}$ is consistent with **RULE 2** for polarization emission where orthogonal mutually accompanying waves, here $\mathbf{\Phi}_{\delta 6}(0°)_{+}$ and $\mathbf{\Phi}_{\delta 7}(90°)$, deterministically combine to produce a state of definite orientation.

Similarly, the δ-form projections $\mathbf{\Phi}_{\delta 8}(0°)$ and $\mathbf{\Phi}_{\delta 9}(90°)$ sum vectorially to give a resultant on path 11

$$\mathbf{\Phi}_{\delta 8}(0°)+\mathbf{\Phi}_{\delta 9}(90°)$$

$$=\xi\cos(\theta)\sin(0°_{\alpha})\mathbf{r}_{\delta}(0°)+\xi\sin(\theta)\sin(0°_{\alpha})\mathbf{r}_{\delta}(90°).$$

$$=\xi\sin(0°_{\alpha})[\cos(\theta)\mathbf{r}_{\delta}(0°)+\sin(\theta)\mathbf{r}_{\delta}(90°)]$$

$$=\xi\sin(0°_{\alpha})\mathbf{r}(\theta)$$

$$=\mathbf{\Phi}_{11}(\theta). \tag{28.4}$$

The LR analysis of the PBS loop demonstrates that the $\mathbf{\Phi}_{10}$ and $\mathbf{\Phi}_{11}$ orientations are identical to that of $\mathbf{\Phi}_{1}$ when $-45°<\theta<+45°$. Moreover, $|\mathbf{\Phi}_{10}|^2+|\mathbf{\Phi}_{11}|^2$ shows that the output wave intensity is conserved relative to the input wave intensity$|\mathbf{\Phi}_{1}|^2$. $\mathbf{\Phi}_{10}(\theta)_{+}$ is occupied and $\mathbf{\Phi}_{11}(\theta)$ is empty.

The corresponding analysis when $+45°<\theta<+135°$ is straightforward. In this case the $\mathbf{\Phi}_{1}(\theta)_{+}$ wave packet arc intersects the horizontal polarization axis of the PBS resulting in the projective condensation of the wave packet onto that horizontal polarization axis along with the resident energy quantum. The horizontal polarization axis of the PBS is then associated with photon transmission. See for example the δ-form path 3 in the Fig. 4(c) depiction of the PBS dielectric. Accordingly, $\mathbf{\Phi}_{\delta 3}(90°)$ is occupied,

$$\mathbf{\Phi}_{\delta 3}(90°)_{+}=\xi\sin(\theta)\,\mathbf{r}_{\delta}(90°)_{+} \tag{29.4}$$

and $\mathbf{\Phi}_{\delta 2}(0°)$ on δ-form path 2 is empty,

$$\mathbf{\Phi}_{\delta 2}(0°)=\xi\cos(\theta)\,\mathbf{r}_{\delta}(0°). \tag{30.4}$$

When $\mathbf{\Phi}_{\delta 3}(90°)_{+}$ exits the dielectric shown in Fig. 12(b), we have again the same form of the wave amplitude on path 5, $\mathbf{\Phi}_{5}(90°_{\alpha})_{+}$, but occupied since the transmitted $\mathbf{\Phi}_{\delta 3}(90°)_{+}$ is itself occupied.

When $\mathbf{\Phi}_{5}(90°_{\alpha})_{+}$ reaches dielectric shown in Fig.12(c), its $90°_{\alpha}$ horizontal orientation satisfies $+45°<90°_{\alpha}<+135°$ and the $\mathbf{\Phi}_{5}(90°_{\alpha})_{+}$ wave arc projectively condenses onto the horizontal polarization axis of dielectric carrying with it the energy quantum onto the δ-form horizontal planar wave amplitude

$$\mathbf{\Phi}_{\delta 7}(90°)_{+}=\xi\sin(\theta)\cos(0°_{\alpha})\,\mathbf{r}_{\delta}(90°)_{+} \tag{31.4}$$

where it joins with the now empty $\mathbf{\Phi}_{\delta 6}(0°)$. Accordingly, we have the same form of the amplitude sum for $\mathbf{\Phi}_{\delta 6}$ and $\mathbf{\Phi}_{\delta 7}$ as before with the only difference being that the energy quantum is provided to the resultant $\mathbf{\Phi}_{10}$ from path 7 instead of from path 6 giving

$$\begin{aligned}
&\mathbf{\Phi}_{\delta 6}(0°)+\mathbf{\Phi}_{\delta 7}(90°)_{+}\\
&= \xi\cos(\theta)\cos(0°_{\alpha})\,\mathbf{r}_{\delta}(0°)+\xi\sin(\theta)\cos(0°_{\alpha})\,\mathbf{r}_{\delta}(90°)_{+}\\
&= \xi\cos(0°_{\alpha})\,[\cos(\theta)\,\mathbf{r}_{\delta}(0°)_{+}+\sin(\theta)\,\mathbf{r}_{\delta}(90°)]\\
&= \xi\cos(0°_{\alpha})\,\mathbf{r}(\theta)_{+}\\
&= \mathbf{\Phi}_{10}(\theta)_{+}.
\end{aligned} \tag{32.4}$$

In summary, returning to the example with $-45°<\theta<+45°$, the loop has an input amplitude

$$\mathbf{\Phi}_{1}(\theta)_{+}=\xi\;\mathbf{r}(\theta)_{+} \tag{33.4}$$

and two output amplitudes, the occupied

$$\mathbf{\Phi}_{10}(\theta)_{+}=\xi\cos(0°_{\alpha})\,\mathbf{r}(\theta)_{+} \tag{34a.4}$$

and the empty

$$\mathbf{\Phi}_{11}(\theta)=\xi\sin(0°_{\alpha})\,\mathbf{r}(\theta). \tag{34b.4}$$

These results for the LR representation show that the unit input wave intensity on $\mathbf{\Phi}_{1}(\theta)_{+}$ is split into a $\cos^2(0°_{\alpha})$ fraction on the occupied $\mathbf{\Phi}_{10}(\theta)_{+}$ and a $\sin^2(0°_{\alpha})$ fraction on the empty $\mathbf{\Phi}_{11}(\theta)$. The proportionality of that split for any particular input photon is determined in a random process by the value of $0°_{\alpha}$ that occurs as the waves emerge from the dielectric layers of the first PBS.

That $0°_\alpha$ value is identified as the bisector orientation of a random member of a 0° polarization ensemble.

The fraction of the wave intensity emergent on the empty $\mathbf{\Phi}_{11}(\theta)$ confirms that wave intensity and ΣI are conserved in LR. In contrast, CI effectively requires the non-local "collapse" of wave intensity in transit to path 11 as well as an instantaneous non-local materialization of that collapsed wave intensity going to path 10.

For CI, the transit of the PBS M-Z loop as a unitary process is understood to relate to the "observable" energy quantum but not to the wave on which it resides as it is for LR.

This distinction is explicitly made manifest in the two outputs of the PBS M-Z loop transit but is not apparent in the simpler single output of the contiguous calcite loop transit.

Notably for LR, the random process associated with the wave transit of the first PBS has no bearing on the output path taken by the energy quantum. That path is deterministically set to be path 10 via path 4 when the objectively real input photon satisfies $-45°<\theta<+45°$ and path 10 via path 5 when the objectively real input photon satisfies $+45°<\theta<+135°$.

Most significantly with respect to the present section, the occupied output wave $\mathbf{\Phi}_{10}(\theta)_+$ on path 10 has the identical θ orientation of the input wave $\mathbf{\Phi}_1(\theta)_+$ on path 1 in a process that does not invoke non-local superposition.

4.5. CI Treatment of Photon Transits of Loops Equipped with Polarization-based Beam Splitting Devices

In the above subsections **4.2.**, **4.3.**, and **4.4.**, we analyzed photon transits of three loops utilizing polarization-based beamsplitters from the perspective of LR. In the present subsection we compactly present a single comparative CI analysis of photon transits for all three of those loops. (In the preceding subsection, **4.1.**, we had analyzed photon transits of a Mach-Zehnder loop equipped with non-polarizing beamsplitters from both perspectives.)

The loop transit analyses for the three loop configurations equipped with polarizer-based beam splitting devices are all fundamentally the same from the perspective of CI. A definite θ linearly polarized state, $|\theta\rangle$ on path 1 is incident on the three loops, Fig's. 7, 9, and 12(a). At incidence, vertical and horizontal projection components $|v\rangle$ and $|h\rangle$ of each photon travel on respective "v" and "h" paths in each loop. Relative to the Fig's 7, 9, and 12 (a), the v and h paths are respectively 2→6 and 3→7 for the Fig. 7 contiguous calcite polarizers with output on 8, 2→2a→6 and 3→3a→7 for the Fig. 9 non-contiguous calcite polarizers with output on 8, and lastly, 4 and 5 for the Fig. 12(a) PBS M-Z with output on 10. The $|v\rangle$ and $|h\rangle$ components acquire amplitude coefficients of cos θ and sin θ as they are respectively projected onto the v and h paths of the various loops.

In summary for those three loop configurations, an incident state $|\theta\rangle$ splits into a non-local superposition state $\cos\theta\,|v\rangle+\sin\theta\,|h\rangle$ on each loop, a process that is reversed to $|\theta\rangle$ as the non-local superposition state arrives at the exit point of each loop giving

$$|\theta\rangle\rightarrow \cos\theta\,|v\rangle+\sin\theta\,|h\rangle\rightarrow|\theta\rangle. \tag{35.4}$$

From the perspective of the positivist-based CI, this compact analysis is justified by the indistinguishability of an output definite linear polarization state |θ⟩ relative to an input definite linear polarization state |θ⟩ and the inability to demonstrate an empty wave on one leg of a loop. That analysis necessarily invokes non-locality and, concurrently, probabilistic non-reality for the photon.

Parenthetically we are reminded that CI regards the input and output states of the respective Fig.'s 7, 9, and 12 loops analyzed in this section to be identically polarized. For CI the assessment of a state's polarization is necessarily statistical in the regard that a large number of state samplings must be acquired in order to compile a representative distribution that identifies the polarization. This statistical evaluation must be applied to the input and output states of those three loops to establish their identical polarizations.

In contrast for LR, identical polarizations of input and output states for Fig. 7 and 12 loops are objectively established from a single input state and its resultant output state since each individual input state is replicated at the output.

For the Fig. 9 loop, because of a loss of correlation on the loop, this process is still effective but can only objectively establish nearly identical polarizations of input and output states from a single input state and its resultant output state.

5. Photon Transits of Loops that Provide Testable Differentiation of CI and LR

In the configurations associated with the foregoing four conventional loop configurations the LR representation self-consistently predicts properties of resultant states that are objectively real but for which the resultant states themselves are not testably distinguishable from the corresponding resultant states predicted by CI. The question arises, 'Do other loop configurations exist for which a self-consistent application of the LR representation predicts objectively real properties of resultant states that render the resultant states testably distinguishable from those of the corresponding CI predicted states?'

From an understanding of the LR analyses of the foregoing conventional loops, we find that we can deduce a variety of novel loop configurations that yield predicted, testable LR output states at variance from the corresponding predicted output states for CI.

Two examples of these novel loop configurations are examined in the subsections below. Notably, these loop configurations depart from the global symmetry of the conventional loops analyzed in the foregoing subsections.

5.1. Analysis of a Loop Configuration for Testing the Reality of LR States

5.1.1. Photon Transits of an Asymmetric PBS M-Z +BS Loop

We begin our analysis with the Fig 13(a) loop that breaks the symmetry of the Fig. 12(a) PBS M-Z loop by the inclusion of a non-polarizing beam splitter inserted on one leg of the loop. As with all loops previously considered here, the optical path lengths of the respective loop legs are equal. That condition ensures that photons emerging from the loops are not elliptically polarized.

The analysis is first presented from the perspective of LR before considering the CI analysis. Vertically polarized photons such as those depicted in Fig. 2 are provided to the input path 1. The amplitudes of these photons can be represented as $\mathbf{\Phi}_1(0°_\mu)_+ = \xi\ \mathbf{r}(0°_\mu)_+$. The beamsplitter with a reflection coefficient r and a transmission coefficient t is inserted on path 4. The amplitude sequence for paths 1→2→4→4a→6 is given by

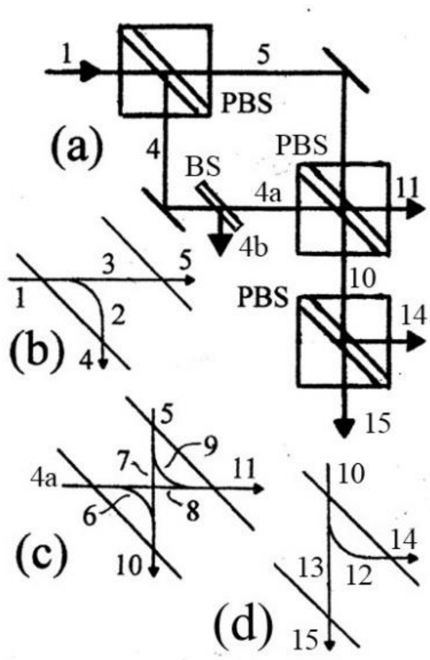

Fig. 13(a-d): Fig. 13(a) shows an asymmetric loop configuration analogous to a PBS M-Z loop, Fig. 12(a), that additionally includes non-polarizing beamsplitter BS on one leg of the loop. That inclusion changes the polarization for a subset of the photons emerging from the loop on path 10 for an LR analysis but not for a CI analysis. Fig.'s 13(b), (c), and (d) show respective PBS dielectric layer transit details.

$$\mathbf{\Phi}_1(0°_\mu)_+ = \xi\ \mathbf{r}(0°_\mu)_+$$

$$\to_{\text{PBS-v}}\ \mathbf{\Phi}_{\delta 2}(0°)_+ = \xi \cos 0°_\mu\ \mathbf{r}_\delta(0°_\mu)_+$$

$$\to_{\text{pol-emit}}\ \mathbf{\Phi}_4(0°_\mu)_+ = \xi \cos 0°_\mu\ \mathbf{r}(0°_\alpha)_+$$

$$\to_{\text{BS-t}}\ \mathbf{\Phi}_{4a}(0°_\mu)_+ = \xi\ t \cos 0°_\mu\ \mathbf{r}(0°_\alpha)_+$$

$$\to_{\text{PBS-v}}\ \mathbf{\Phi}_{\delta 6}(0°)_+ = \xi\ t \cos 0°_\alpha \cos 0°_\mu\ \mathbf{r}_\delta(0°_\mu)_+ \tag{1.5}$$

where Eq. (1.5) applies to the photon transits at the beamsplitter BS in which the energy quantum on path 4 randomly ascends onto the transmitted LR wave on path 4a rather than onto the reflected LR wave on path 4b. The latter outcomes occur for an r^2 fraction of loop-incident photons and are not of interest in this analysis.

The corresponding amplitude sequence for paths 1→3→5→7 in the present analysis is

$$\mathbf{\Phi}_1(0°_\mu)_+ = \xi\ \mathbf{r}(0°_\mu)_+$$

$$_{\text{PBS-h}}\ \mathbf{\Phi}_{\delta 3}(90°)= \xi \sin 0°_\mu\ \mathbf{r}_\delta(90°)$$

$$\rightarrow_{\text{pol-emit}}\ \mathbf{\Phi}_5(90°_\alpha)= \xi \sin 0°_\mu\ \mathbf{r}(90°_\alpha)$$

$$\rightarrow_{\text{PBS-h}}\ \mathbf{\Phi}_{\delta 7}(90°) = \xi \sin 90°_\alpha \sin 0°_\mu\ \mathbf{r}_\delta(90°_\mu)= \xi \cos 0°_\alpha \sin 0°_\mu\ \mathbf{r}_\delta(90°_\mu). \quad (2.5)$$

The states $\mathbf{\Phi}_{\delta 6}(0°)_+$ and $\mathbf{\Phi}_{\delta 7}(90°)$ respectively in the sequences of Eq's. (1.5) and (2.5) provide the vertically and horizontally oriented planar LR states in the second PBS that vectorially combine to deterministically generate a resultant polarizer emission state on path 10.

That resultant state is

$$\mathbf{\Phi}_{10+}= \mathbf{\Phi}_{\delta 6}(0°)_+ + \mathbf{\Phi}_{\delta 7}(90°)$$

$$= \xi\ t \cos 0°_\alpha \cos 0°_\mu\ \mathbf{r}_\delta(0°_\mu)_+ + \xi \cos 0°_\alpha \sin 0°_\mu\ \mathbf{r}_\delta(90°_\mu)$$

$$= \xi \cos 0°_\alpha\ [t \cos 0°_\mu\ \mathbf{r}_\delta(0°_\mu)_+ + \sin 0°_\mu\ \mathbf{r}_\delta(90°_\mu)]. \quad (3.5)$$

Aside from the inclusion of the t cofactor, the above expression for $\mathbf{\Phi}_{10+}$ is otherwise identical to that for $\mathbf{\Phi}_{10+}$ in subsection **4.4** where θ specifies a particular vertical polarization orientation in analogy to the $0°_\mu$ in the above Eq. (3.5).

Our particular interest here with respect to $\mathbf{\Phi}_{10+}$ is the orientation of that resultant vector amplitude as a function of the orientation $0°_\mu$ of the incident state $\mathbf{\Phi}_1(0°_\mu)_+$. In that regard we focus on the sum of the vertical and horizontal vectors bracketed in Eq. (3.5) where the vertical vector has a magnitude of $t \cos 0°_\mu$ and the horizontal vector has a magnitude of $|\sin 0°_\mu|$. The $0°_\mu$ orientations of the incident states have a range of −45° to +45° but for clarity of analysis we first examine the subrange of 0° to +45° without loss of generalization.

The effect of the attenuation of the vertical vector by a factor t can now be appreciated. In the absence of the beamsplitter BS, $t\rightarrow 1$ and the relative vertical and horizontal vector magnitudes, respectively $\cos 0°_\mu$ and $\sin 0°_\mu$, produce a resultant vector orientation that trivially replicates the orientation of the loop-incident state as shown in Eq.'s (33.4) and (34a.4). The incident vertically polarized states are each simply replicated to identically oriented vertically oriented states which includes the particular incident state at the terminus of the subrange 0° to +45° where the marginally vertically polarized incident state orientation is $0°_\mu$=+45°. The resultant output orientation is of course +45° because the vertical and horizontal vector magnitudes are equal, i.e. $\cos(+45°)= \sin(+45°)$, and that terminus state is also marginally vertically polarized when $t\rightarrow 1$.

However, with any beamsplitter BS present, the cofactor $t<1$ in Eq. (3.5) attenuates the vertical vector magnitude by t. The vector amplitude equality condition, in which vertical polarization for the output state still occurs, is necessarily at some critical orientation $\theta_c=0°_\mu<45°$ of the incident state. That $\theta_c<45°$ can be determined from the expression

$$t \cos \theta_c= \sin \theta_c. \quad (4.5)$$

At that critical incident state orientation θ_c the horizontal vector magnitude exactly equals the vertical vector magnitude and marginally still results in a vertically polarized loop-output state. Importantly, any incident states with $0°_\mu>\theta_c$ result in loop output states that are horizontally polarized, i.e. they have orientations in the subrange +45° to +135°. If the loop-incident states are photons, i.e. states bearing energy quanta, a self-consistent assignment of energy quanta on loop states deterministically ensures that those horizontally polarized output states are also photons.

It would be tempting to identify these horizontally polarized states as members of a horizontally polarized ensemble with orientations given by $90°_\mu$ and indeed the orientations of those states can be identified as having the orientations of particular members of a horizontal polarization ensemble represented by $90°_\mu$.

Moreover, while the remaining output states generated from input state orientations $0°_\mu<\theta_c$ are still vertically polarized, it is similarly tempting to represent the orientations of those output states by $0°_\mu$. As in the case of the horizontally polarized states, the remaining vertically polarized output states can be identified as having the orientations of particular members of a vertical polarization ensemble represented by $0°_\mu$.

However, the collective path 10 output states of the Fig. 13 loop constitute a new ensemble that is fundamentally distinct from the conventional linear polarization ensemble of states which for CI is a definite linear polarization "state."

That new ensemble is most instructively understood by examining a particular example. In that regard any t value would in principle suffice. Nevertheless, in the interests of examining an example that is both graphically visualizable and experimentally definitive we choose a t=0.447 corresponding to the transmission coefficient for a lossless 80:20 R/T beamsplitter. (Non-polarizing dielectric-based beamsplitters closely approximate lossless performance.) In that choice we lose 80% of the loop-incident photons by reflection at the beamsplitter but that loss is of no consequence in our analysis of the remaining 20% exiting the loop on path 10. With that choice, from Eq. (4.5)

$$\theta_c=24.1° \tag{4.6}$$

for the 80:20 beamsplitter.

For an incident state orientation $0°_\mu< 24.1°$ the vertical vector magnitude still exceeds the horizontal vector magnitude and the resultant vector orientation, which is also the orientation of $\mathbf{\Phi}_{10+}$, is less than 45°. For those $0°_\mu< 24.1°$ there is a sub-distribution of $\mathbf{\Phi}_{10+}$ output states that are vertically polarized.

Conversely, for incident state orientations $0°_\mu>24.1°$ the horizontal vector magnitude exceeds that of the vertical vector and there is a complementary sub-distribution of $\mathbf{\Phi}_{10+}$ output states that are horizontally polarized.

From these deterministic boundaries of the sub-distributions we can readily determine the relative fractions of $\mathbf{\Phi}_{10+}$ states that are in the two sub-distributions by an inspection of the Fig. 2 15-member ensemble distribution. In the present context that Fig. 2 distribution can be understood to correspond to the distribution of incident states $\mathbf{\Phi}_1(0°_\mu)_+$ since each of those

$\mathbf{\Phi}_1(0°_\mu)_+$ states at some particular $0°_\mu$ orientation one-for-one deterministically transfers its energy quantum to a $\mathbf{\Phi}_{10+}$ state that is either in the vertically polarized sub-distribution or in the horizontally polarized sub-division based upon the value of its $0°_\mu$ orientation relative to θ_c=+24.1°. Since we need to determine the relative fractions of $\mathbf{\Phi}_{10+}$ states that are respectively in the two sub-distributions, this task can be accomplished by counting the relative fractions of $\mathbf{\Phi}_1(0°_\mu)_+$ states that contribute respectively to the vertically polarized sub-distribution and to the horizontally polarized sub-distribution.

On the right side of the Fig. 2 distribution of vertically polarized ensemble members, corresponding to subrange of $0°_\mu$ over 0° to +45°, we examine members with arc bisector orientations that exceed θ_c. A vertical line placed at θ_c=+24.1° intersects the 90° arcs of all those members as well as the arcs of some other members that should be excluded because they have bisector orientations to the left of θ_c. That exclusion is facilitated by a second vertical line placed at +24.1°+45°=+69.1° that intersects only the arcs of the sub-distribution of ensemble states that have bisector orientations that lie to the right of θ_c. Over the present subrange of incident orientations from 0° to +45° the sub-distribution of ensemble states with orientations greater than θ_c is simply

$$\cos^2 69.1°=0.1273 \tag{5.5}$$

in the limit N=15→∞ for Fig. 2.

By symmetry, an equivalent analysis applied to the subrange of incident orientations from 0° to −45° similarly yields the sub-distribution of incident ensemble states with orientations less than $-\theta_c$ as 0.1273.

A single sub-distribution combining these two sub-distributions represents a 0.255 fraction of photons incident on the second PBS that emerge as horizontally polarized photons on $\mathbf{\Phi}_{10+}$. Correspondingly, there is a complementary sub-distribution that represents a 0.745 fraction of photons incident on the second PBS that emerge as vertically polarized photons on $\mathbf{\Phi}_{10+}$.

These results show that the distribution of photon states associated with $\mathbf{\Phi}_{10+}$ is "bimodal." The distribution consists of two mutually distinct sub-distributions of photon states. Those photon states can be separated from path 10 by a polarization device such as the third PBS in Fig. 13 yielding 25.5% of those photon states as horizontally polarized on path 15 and 74.5% of those photon states as vertically polarized on path 14.

With the numerical choice of t, we can now generate a finite-member distribution of the bimodal ensemble that can be contrasted to that of Fig. 2 which may be regarded as the incident ensemble. Proceeding with an N=15 member ensemble as in Fig. 2, the centermost α=8 state is trivially unaltered from that in Fig. 2 by symmetry. That α=8 state has an ensemble orientation $0°_{8bm}$=0°. The appended subscript "bm" identifies the $0°_{\alpha bm}$ ensemble as the currently examined bimodal ensemble as distinguished from the corresponding conventional linear polarization ensemble $0°_\alpha$. The determination of the remaining 14 orientations $0°_{\alpha bm}$ is a straightforward two-step process.

1. Calculate the arc bisector orientation $0°_\alpha$ of each remaining α incident state in the N=15 Fig. 2 ensemble distribution using Eq. (15.2). Symmetry reduces the remaining calculations to seven.

2. Each $0°_{\alpha bm}$ is the orientation of a vector resultant from the sum of vertical vector of magnitude t cos $0°_\alpha$ and a horizontal vector of magnitude sin $0°_\alpha$. See Eq. (3.5). Then with t=0.477

$$0°_{\alpha bm} = \tan^{-1} [\sin 0°_\alpha / (0.447 \cos 0°_\alpha)]. \quad (6.5)$$

From the full set of $0°_{\alpha bm}$ orientations, the left and right extents of the associated arc spans are simply $0°_{\alpha bm} \pm 45°$. The 15 bimodal ensemble states are plotted in Fig. 14. Selected associated numerical values for the α=1, 2, and 3 states are examined here.

For α=1, where the incident α=1 orientation $0°_1$=45°, $0°_{1bm}$=65.915° and the arc span extends from 20.915° to 110.915°. This state is effectively rotated by almost +21° relative to the corresponding incident α=1 state. The righthand envelope of the bimodal ensemble extends to 110.915° compared to 90° for the conventional polarization ensemble. The lefthand extent of the arc span does not intersect the vertical axis but does intersect the horizontal axis, clearly identifying the α=1 state as horizontally polarized.

For α=2, the associated α=2 incident state orientation $0°_2$=29.5° is several degrees larger than the critical orientation θ_c=24.1° which indicates that the orientation $0°_{2bm}$ of the α=2 bimodal ensemble state is now horizontally polarized. This is confirmed upon calculating the arc bisector orientation $0°_{2bm}$ = 51.69° which shows that the horizontal axis is intersected by the right portion of that arc span extending to +51.69+45°= +96.69°.

For α=3, the associated α=3 incident state orientation $0°_3$=22.79° is marginally 1.29° smaller than the critical orientation θ_c=24.1° which indicates that the orientation $0°_{3bm}$ of the α=3 bimodal ensemble state is marginally still vertically polarized. This is confirmed upon calculating the arc

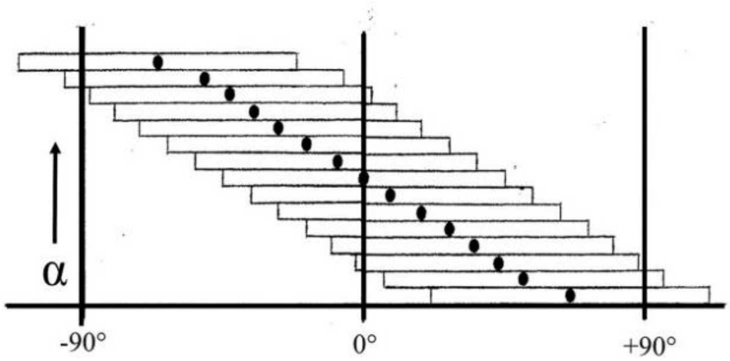

Fig. 14: A bimodal output ensemble predicted by LR for the Fig. 13 loop where t^2=0.2 for the BS. The ensemble is depicted by a finite-member distribution of N=15 states. States α=1, 2, 14, and 15 are horizontally polarized and the remaining are vertically polarized giving a bimodal ratio of 4:11. A bimodal output ensemble is contrary to the CI prediction for that loop.

bisector orientation $0°_{2bm}$=43.21° which shows that the vertical axis is marginally intersected by the left portion of that arc span extending to 43.21°−45°= −1.79°.

Clearly, the single most consequential numerical value to be deduced from the bimodal ensemble is the relative proportion of bimodal states that are horizontally polarized. As shown above for the coarse 15-member incident ensemble, the α=1 and 2 members of that incident ensemble have orientations $0°_\alpha$ larger than θ_c=24.08° resulting in horizontal polarization for the corresponding α=1 and 2 members of the bimodal ensemble. By symmetry, that condition also applies to α=15 and 14. Consequently, the proportion of horizontally polarized states for the bimodal ensemble deduced from the incident N=15 member ensemble is simply 4/15=0.267. This result comports closely with the exact solution given above as 0.255 by symmetry doubling of the Eq. (5.5) result and demonstrates the utility of analyzing individual LR states with the use of a relatively coarse N=15 member ensemble approximation to an N=∞ member ensemble.

We turn finally to the corresponding CI representation of photon transits of the Fig. 13 loop. For that transit we prepare incident photons on path 1 in a definite vertical polarization state. The CI representation is compactly expressed as

$$
\begin{aligned}
1|v\rangle_1 &\rightarrow_{PBS} 1|v\rangle_4 + 0|h\rangle_5 \\
&\rightarrow r\,|v\rangle_{4b} + t\,|v\rangle_{4a} + 0|h\rangle_5 \\
&\rightarrow r\,|v\rangle_{4b} + t\,|v\rangle_{10} + 0|h\rangle_{10}
\end{aligned}
\tag{7.5}
$$

In agreement with the LR analysis, Eq. (7.5) similarly predicts that r^2 of the observable photons emerge on the BS output path 4b and the other t^2 of the observable photons exit the loop on path 10 of the second PBS. However, CI represents those photons output on path 10 entirely as in a definite vertical linear polarization state unlike the LR analysis.

Parenthetically we note that the Fig. 13 loop configuration predicts a novel useful application of interaction-free measurement, IFM, from the perspective of LR. The presence of an opaque object inserted on path 5 can be determined completely free of photon interactions with the object by the total absence of horizontally polarized photons emerging onto path 10. In a minor variation of that IFM application, cross-sectional images of non-opaque objects can be acquired non-destructively using empty wave attenuation by laterally shifting the object through path 5 while concurrently monitoring the relative flux of horizontally polarized photons on path 10. It may also be appreciated that the application of communication with empty waves along path 5 is similarly consistent with the above LR analysis of Fig. 13 loop transits. This capability is most simply demonstrated by conventionally either blocking or unblocking the flow of empty waves emerging from the first PBS in Fig. 13 onto path 5 during some brief time interval Δt. The resultant non-detection or detection of horizontally polarized photons on path 10 during any Δt constitutes either a digital “zero” or a digital “one” respectively. These and other related applications are consistent with LR but are not representable with CI.

5.1.2. The Underlying Basis for the Discrepancy Between the LR Outcomes and the CI Outcomes for Photon Transits of the Loop

For the presently considered Fig. 13 asymmetric PBS M-Z+BS loop the outcomes from the perspective of LR are in discrepancy with those of CI for a sub-distribution of incident LR states. In contrast the Fig. 12 symmetric PBS M-Z loop yields LR and CI outcomes in mutual agreement for all incident LR states albeit with the imposition of probabilistic non-local superposition for the CI "states." The underlying basis for that discrepancy in the presently considered loop can now be understood in detail that reveals the most fundamental insights regarding the differences between the LR and CI representations.

That underlying basis begins with the CI representation of the definite 0° linearly polarized definite "state" incident on the Fig. 13 loop. The interaction of that "state" with the first PBS immediately confers amplitude cofactors of 1 and 0 onto the paths 4 and 5, respectively. The inserted BS on path 4 serves only to reduce the amplitude on path 4a by a t cofactor. The subsequent interaction of the path 4a and path 5 amplitudes in the second PBS predictably yields a vertically polarized output state on path 10.

From the perspective of LR, the incident definite 0° linearly polarized "state" is not a single photon state but a statistical distribution of LR states represented by an ensemble such as that depicted in Fig. 2. That ensemble distribution is symmetrical about 0°. For LR, the singular center-most member occurs at some value of μ=n (where n=7 for the N=15 ensemble) and

$$\mathbf{\Phi}_1(0°_n)_+ = \mathbf{\Phi}_1(0°)_+. \tag{8.5}$$

Essentially, only that centermost member of the entire ensemble has an objectively real bisector orientation of 0°. Notably that is the orientation that CI applies to the 0°-polarized definite photon "state" in representing, from an LR perspective, the statistical ensemble of all constituent, objectively real LR states.

Out of the entire ensemble that singular $\mathbf{\Phi}_1(0°_n)_+$ member will deterministically always result in a vertically polarized LR output state on path 10 because the amplitude cofactor conferred onto path 5 is exactly 0 for that μ=n member alone. Even if the BS beamsplitter transmission horizontal transmission coefficient t is reduced to near zero by inserting a BS with 0<t<<1, the cofactor on path 4a is very small but still non-zero and the corresponding LR resultant state on path 10 is always still identified as vertically polarized. However, in that near zero limit, virtually all the remaining incident ensemble states $\mathbf{\Phi}_1(0°_\mu)_+$, where μ≠n, result in cofactors on path 5 that exceed the near-zero cofactors on path 4a and all of those states emerge on path 10 as horizontally polarized.

In contrast for CI, where the linear polarization "state" is regarded as irreducible, constituent fundamental states within that definite state must be excluded. By that self-consistent exclusion, the definite 0°-polarized state confers a 0 amplitude cofactor onto path 5 that deterministically results in a vertically polarized state on path 10 which is the same result as that for LR in the singular case of μ=n for the incident LR state.

It can then be appreciated that the present discrepancy between CI and LR arises because of the asymmetry of the Fig. 13 PBS M-Z loop. For LR that asymmetry sufficiently reduces the amplitude cofactors of LR states on path 4a such that, in vectorial combination with states having non-zero cofactors on path 5, a sub-distribution of LR output states on path 10 are horizontally polarized.

For CI, no such sub-distribution can arise or is even representable in an interpretation where the "state" constitutes a complete, irreducible representation of the photon. The CI linear polarization "state" cannot in principle admit reducible entities such as the horizontally polarized sub-division of states on path 10 predicted by LR. Those LR reducible entities, objectively real empty waves, are explicitly responsible for generating the bimodal output distribution of waves on path 10.

5.2. Analysis of Loop Configurations that Image the Transverse Structure of LR Photon States

In this subsection we examine loop configurations for which a self-consistent application of LR predicts output states that effectively image the transverse structure of individual photon wave packets.

This imaging process can be demonstrated by either of the two closely related loop configurations depicted in Fig.'s 15 and 16(a). These configurations differ by their respective output components, a two-channel polarizer such as calcite and a polarizing beam splitter but the configurations are functionally equivalent. Because of that functional equivalency, we can conveniently track the progressive states in each loop with the same path numbering for both configurations.

Fig.'s 15 and 16(a) both depict loops receiving vertically polarized photons on path 1. The photons are input to a non-polarizing beamsplitter which we choose to be 50:50 for the present analysis. For both configurations, the optical path lengths of the loop legs are set equal however one leg of the Fig. 16(a) configuration is then shifted by half a wavelength to compensate for an unequal number of device-induced 180° phase shifts on the legs of the Fig. 16(a) loop.

The LR analysis of the Fig.'s 15 and 16(a) configurations are conducted by considering an objectively real member of the input vertical polarization ensemble. That member has an orientation (arc bisector) at some θ where $-45°<\theta<+45°$.

We track the outcome of that single objectively real member. On path 1

$$\mathbf{\Phi}_1(\theta)_+ = \xi\, \mathbf{r}(\theta)_+ \tag{9.5}$$

where $\mathbf{r}$ is a unit radial vector in the transverse plane oriented at θ. The path 2 states are

$$\mathbf{\Phi}_2(\theta)= \xi\, (\sqrt{2}/2)\, \mathbf{r}(\theta), \tag{10.5}$$

and the path 3a→3b states are

$$\mathbf{\Phi}_{3a}(\theta)= \xi\, (\sqrt{2}/2)\, \mathbf{r}(\theta)$$

$$\rightarrow_{\mathrm{HWPs}}\ \mathbf{\Phi}_{3b}(\theta+90°)= \xi\ (\sqrt{2}/2)\ \mathbf{r}(\theta+90°). \tag{11.5}$$

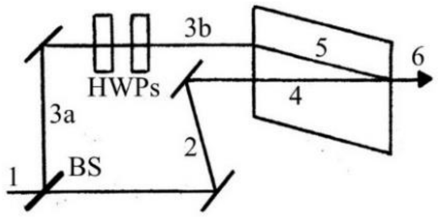

Fig. 15: A loop configuration for splitting the amplitude of a vertically polarized photon to produce a super polarized output state from a calcite polarizer. That output state is oriented at 45° independent of the particular orientation of the incident photon state.

We note that in the above Fig's. 15 and 16(a) loop configurations the second HWP, which is oriented at 90°, could be omitted. This omission would not result in the 90° rotation of the LR state that had been on path 3a but would instead result in the mirror image of the 90° rotated state on path 3b about the horizontal axis of the polarizer. The resultant projection coefficient cos(−θ) is mathematically the same as the cos θ coefficient that occurs with the inclusion of the second HWP. In any case, the inclusion of the second HWP is preferred in the interest of generating an objectively real orthogonal rotation of LR states on path 3a.

We shall shortly see that the entire loop transit process is independent of the particular loop leg randomly taken by the energy quantum of the input photon. Accordingly, on the states intermediate to the input state $\mathbf{\Phi}_1$ and the output state $\mathbf{\Phi}_6$ the occupation specification "+" is omitted.

States $\mathbf{\Phi}_2$ and $\mathbf{\Phi}_{3b}$ proceed on paths 4 and 5 as the planar wave states

$$\mathbf{\Phi}_{\delta 4}(0°)= \xi\ (\sqrt{2}/2)\cos\theta\ \mathbf{r}_{\delta}(0°) \tag{12.5}$$

and

$$\mathbf{\Phi}_{\delta 5}(90°)= \xi\ (\sqrt{2}/2)\sin(\theta+90°)\ \mathbf{r}_{\delta}(90°) = \xi\ (\sqrt{2}/2)\cos(\theta)\ \mathbf{r}_{\delta}(90°). \tag{13.5}$$

Adding these states vectorially yields an output state on path 6.

$$\begin{aligned}\mathbf{\Phi}_{\delta 4} + \mathbf{\Phi}_{\delta 5} &= \xi \cos\theta\ \mathbf{r}(45°)_{+}\\ &=\mathbf{\Phi}_6(45°)_{+}.\end{aligned} \tag{14.5}$$

The output states in Fig. 15 and 16 (a) configurations are functionally identical. Both cases show that an arbitrarily oriented input member of a vertically polarized ensemble is mapped to a 45° orientation. $\mathbf{\Phi}_6(45°)_{+}= \xi \cos\theta\ \mathbf{r}(45°)_{+}$ is a single objectively real photon generated on the output path 6 of the Fig. 15 and 16 (a) configurations from a single objectively real input photon state $\mathbf{\Phi}_1(\theta)_+ = \xi\, \mathbf{r}(\theta)_+$ that has an orientation θ where −45°<θ<+45°.

A subsequent input photon state $\mathbf{\Phi}_1(\theta')_+ = \xi\, \mathbf{r}(\theta')_+$ that has an orientation θ′ generally distinct from θ, similarly results in an output state $\mathbf{\Phi}_6(45°)_+ = \xi \cos\theta'\, \mathbf{r}(45°)_+$ when −45°<θ′<+45°.

Most generally a θ-oriented input state is manipulated by the Fig's. 15 and 16 loop configurations to always emerge as an LR 45°-oriented output state that can summarily be expressed by the sequence

$$\mathbf{\Phi}_{in}(\theta)_+ = \xi\, \mathbf{r}(\theta)_+ \rightarrow \mathbf{\Phi}_{out}(45°)_+ = \xi \cos\theta\, \mathbf{r}(45°)_+. \quad (15.5)$$

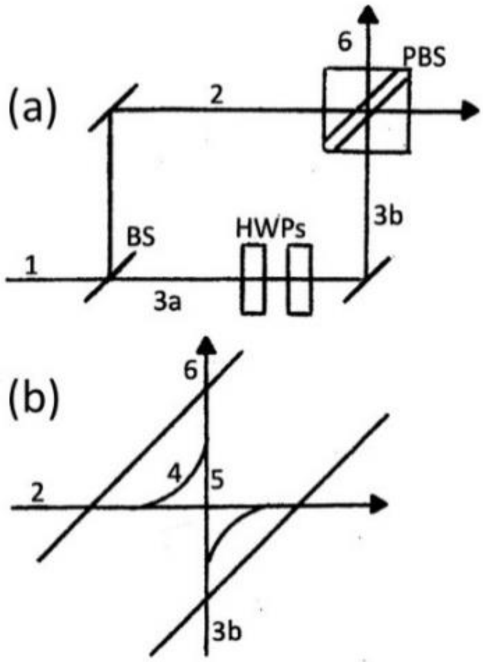

Fig. 16(a,b): (a) depicts a loop configuration functionally equivalent to Fig. 15 but using a PBS instead of calcite to produce a super polarized photon oriented at 45°. (b) is a detail of beam paths in the PBS dielectric layer.

This is a fully deterministic outcome consistent with the same principles employed in other fully deterministic outcomes such as those associated with the Fig's. 7 and 12 loops.

All the subsequent input photons result in output photons that have identical orientations of 45° and differ only by the cosine amplitude coefficient that each acquires as objectively real members of the vertically polarized ensemble of input photons. Those coefficients range from 0.707 to 1 and do not differentially distinguish the various output photons on path 6 with regard to measurement by a rotatable polarizer and a detector. In this regard, the identically oriented output photons are appropriately identified as "super polarized."

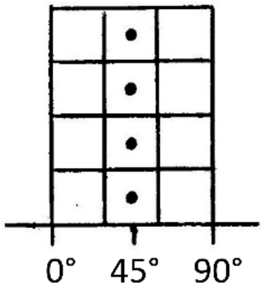

Fig. 17 A symbolic angularly partitioned ensemble of "super polarized" photons oriented at 45°. Four members are depicted but since all members are identically oriented, a single photon would constitute a minimally representative ensemble distribution.

For a sampling of four input photons, Fig. 17 is a symbolic representation of the distribution of the four corresponding super polarized photon states output onto path 6 from the LR analysis. Fig. 18 depicts the corresponding vector representation of those states.

A clockwise rotating polarizer oriented at θ receiving a beam of these 45°-oriented super polarized photons is predicted to yield step function full transmission beginning at 0° continuing uniformly to a complementary non-transmission of the step function at 90°. In that process the transverse structure of the photon wave packet is effectively imaged.

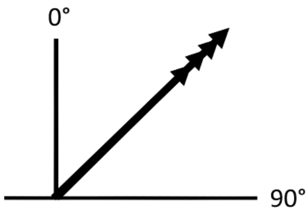

Fig. 18: The symbolic vector diagram representing the super polarized ensemble depicted in Fig. 17.

We next examine the states from the perspective of CI. The non-polarizing beam splitter divides the input state $|v\rangle_1$ on path 1 into $(\sqrt{2}/2)|v\rangle_2$ on path 2 and $(\sqrt{2}/2)|v\rangle_{3a}$ on path 3a. Two consecutive HWP's on path 3a rotate the vertically polarized path 3a state to the horizontally polarized state on path 3b, $(\sqrt{2}/2)|h\rangle_{3b}$. The states on paths 2 and 3b combine (either in the calcite polarizer or the PBS) to yield a path 6 output state

$$(\sqrt{2}/2)|v\rangle_2 + (\sqrt{2}/2)|h\rangle_{3b} = |d\rangle_6. \tag{16.5}$$

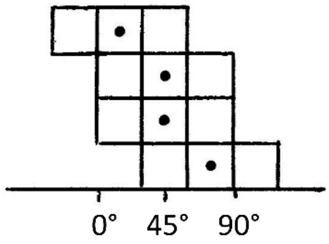

Fig. 19: A symbolic angularly partitioned representation of a 45°-linear polarization ensemble.

CI unremarkably predicts a definite 45°-polarization state for photons on path 6. A rotatable polarizer intercepting the path 6 photons should then yield a characteristic cosine squared transmission probability distribution centered at 45°.

The CI predictions for the path 6 output states are symbolically represented by the Fig. 19 45°-polarization ensemble and the associated Fig. 10 vector diagram.

The CI-predicted Fig. 19 linear polarization distribution is experimentally distinguishable from the LR-predicted Fig. 17 linear polarization ensemble distribution with a rotatable plate polarizer and a detector. The Fig. 19 distribution is recognized as a common diagonally (45°) polarized ensemble of photons whereas the Fig. 17 distribution represents objectively real "super polarized" photons all oriented at 45°.

It can be appreciated that the essence of the above super polarization process resolves to splitting a photon wave oriented at some θ into two waves of equal magnitude still oriented at that θ and then rotating the orientation of one of those waves by 90°. When those two waves each respectively encounter a channel in a two-channel polarizer, the respective vector projections along the vertical axis and horizontal axis of the polarizer are equal and add to an output vector at 45° independent of the orientation of the input photon. Super polarizations to orientations other than 45° are achieved by using a BS with a reflection:transmission ratio other than 50:50.

The super polarization process is dependent upon the LR objectively real structures of photons that are inherently inadmissible and not representable in CI.

Recall that for the Fig. 7 and 12 loops, LR shows that input states are replicated one-for-one at the outputs. In the above we have self-consistently applied the same principles used to analyze LR states traversing those loops to show how any objectively real input state at some θ associated with an input vertically polarized photon, can be deconstructed and reconstructed to give an LR state precisely at 45° or any other selected orientation.

With regard to applications, the capability of imaging photon transverse structure constitutes a notable fundamental investigative application predicted by LR but not representable under CI. Other applications relate to existing scientific and technological applications that are consistent with CI but are potentially improved from the perspective of LR. Most generally these existing applications utilize polarization-dependent interactions with linearly polarized photons incident on a target material, e.g. polarimetry, quantum key distribution (QKD), image display systems, and polarization-sensitive optical coherence tomography (OCT). These existing applications relate to an optimal differential effect of interest when the linear polarization axis of the incident photons has some particular orientation compared to an orientation orthogonal to that particular orientation.

From the perspective of LR, the magnitude of the effect is attributable to the distribution of orientations in an ensemble of linearly polarized photons where the effect originates primarily from the orientations of the member at the distribution centroid and of nearby members. Members with orientations angularly progressively more distal from the centroid have orientations approaching 45° from the centroid. Those distal members may be expected to dilute the magnitude of the differential effect of interest. In such circumstances the use of super polarized photons has the potential to maximize the magnitude of the differential effect of interest and optimize applications currently using linearly polarized photons.

6. Conclusions

A rigorously self-consistent locally real representation, LR, is derived from the underlying quantum mechanical formalism. The LR representation is distinct from the probabilistic Copenhagen Interpretation, CI, of that formalism. Applied to the structure of photons, LR treats the usual longitudinal wave function as an objectively real physical structure that is “completed” to a three-dimensional structure by the inclusion of the objectively real transverse structure derived from that formalism. [1] and [7] The “hidden variables” that complete that structure emerge as structural parameters of the wave, i.e. the longitudinal amplitude, the transverse arc bisector orientation, and the transverse arc span. The objective existence of those variables would be consistent with novel experimental outcomes predicted for photon transits of loops depicted in Fig’s. 13, 15, and 16.

In LR the “hidden” variables are not hidden. Those variables are experimentally measurable. The empty wave amplitude on one leg of the Fig. 13 loop can be measured relative to the wave amplitude on the other loop leg by varying the beamsplitter transmission coefficient t and assessing the respective ratios of vertically polarized photons and horizontally polarized photons emerging from the loop. Similarly, the transverse arc bisector orientation can be measured by varying the beamsplitter transmission coefficient t for the Fig. 15 and 16 loops and observing the respective arc bisector orientations of the super polarized waves. In that process the full complement arc span is also measured.

From the perspective of LR, the set of arc spans for correlated photons has already been measured in Bell experiments. LR shows that it is incorrect to interpret that respective members of correlated pairs are related by being in the same linear polarization state. Because the pairs arise in free space the members must conserve angular momentum by having identical orientations. A sin (2θ) ensemble envelope for one member of the pair emerges from the underlying quantum formalism. That envelope provides the distribution of arc spans for that member. The measured joint probabilities of performed Bell experiments are in agreement with that distribution.

The variables associated with LR provide a completed wave structure that constitutes the basis for locally real states. The LR representation is inherently not subject to Bell's inequality, [2] is in agreement with performed tests of Bell's inequality such as [3-4], and is not disproven by performed tests designed to refute particular locally real representations [6]. Moreover, the LR representation is fully consistent with classical principles of causality as well as the underlying quantum formalism from which it is derived. [1]

The LR locally real states are applied here in the analyses of correlated photons in Bell experiments and photon transits of commonly encountered optical loop configurations. These phenomena, necessarily associated with non-locality under CI, are represented by the LR locally real states without invoking non-local entanglement and superposition. In the analyses of these phenomena, the LR predicted measurable results, while fully in agreement with those of CI, do not provide the means to testably distinguish between CI and LR.

That impasse of distinguishing between CI and LR is addressed here. Multiple novel loop configurations have been deduced from LR that can testably distinguish between CI and LR. Two of those novel loop configurations are presented here.

The first of those two novel loop configurations is essentially a PBS Mach-Zehnder loop with an amplitude diminishing beamsplitter inserted on one loop leg. LR predicts that the loop effectively stretches a CI 0° definite linear polarization state, producing in that process an experimentally measurable bimodal ensemble distribution of LR states that necessarily includes both vertically and horizontally polarized LR states. That bimodal ensemble distribution is not consistent with or representable by CI.

The second novel loop configuration is shown in two closely related variants. A self-consistent implementation of the LR locally real states predicts that randomly oriented incident states are disassembled and reassembled to a single selectable identical orientation, producing in that process an output of "super polarized" photon states with experimentally measurable 90° arc spans that similarly are not consistent with or representable by CI.

The LR predicted outcomes of those two novel loop configurations are shown to provide the basis for multiple consequential applications.

The concordance of LR with a variety of phenomena such as correlated photons and common loop transits does not "prove" the validity of LR. Nor can any such concordance prove the validity of any physical theory. The utility of a physical theory must be assessed on its concordance with known phenomena, its predictive ability for new phenomena and the falsifiability of that theory. [8]

References

[1] S.G. Mirell, "Locally Real States of Photons and Particles", Phys. Rev. A, **65**, 2002, Article ID: 032102/1-22 March (2002).

[2] J.S. Bell, "On the Einstein Podolsky Rosen Paradox", Physics, **1**, No. 3, 1964, 195-200.

[3] S.J. Freedman, and J.F. Clauser, "Experimental test of local hidden-variable theories", Phys. Rev. Lett., **28** (938): 938-941. (1972).

[4] A. Aspect, J. Dalibard, and G. Roger, "Experimental Test of Bell's Inequalities Using Time-Varying Analyzers", Phys. Rev. Lett., **49**, No. 25, 1982, pp. 1804-1807.

[5] J.F. Clauser, and M.A. Horne, "Experimental Consequences of Objective Local Theories". Phys. Rev. D, **10**, No. 2, 1974, 526-535.

[6] M. Genovese, "Research on hidden variable theories: A review of recent progresses", Physics Reports **413**, 2005, pp.319-396 , p 358 and 398; M. Genovese, "Research on hidden variable theories: A review of recent progresses", arXiv:quant-ph/01071 v1 12 Jan 2007, https://doi.org/48550/arXiv.quant-ph/0701071, p 50 and 95.

[7] A. Einstein, B. Podolsky, and N. Rosen, "Can Quantum Mechanical Description of Physical Reality be Considered Complete?", Phys. Rev., **47**, No. 10, 1935, 777-780.

[8] K. R. Popper, *Quantum Theory and the Schism in Physics,* (Rowman and Littlefield, Totowa, NJ, 1982)